ABSTRACT

Controls on the Accumulation of Organic Matter
in the Eagle Ford Group, Central Texas, USA

Kenneth S. Boling, M.S.

Chairperson: Stephen I. Dworkin, Ph.D.

The Upper Cretaceous Eagle Ford Formation is an organic rich marine mudrock which outcrops across central Texas. This study documents the chemostratigraphic character of the Pepper and Eagle Ford Formations in central Texas using major and trace elements, organic matter abundance, and the isotopic and stoichiometric character of organic matter. The chemical data allow the identification of six distinct chemofacies that are potentially useful for correlation purposes. Based on these data, changing paleoceanographic conditions were documented ranging from normal marine conditions associated with the Pepper Formation, anoxic conditions associated with the Lower Eagle Ford Formation, suboxic conditions associated with most of the upper Eagle Fords, and then a return to normal marine conditions at the top of the Eagle Ford Formation. The high TOC content of the lower Eagle Ford was most likely caused by high productivity which in turn drove conditions to anoxia.

Controls on the Accumulation of Organic Matter
in the Eagle Ford Group, Central Texas, USA

By

Kenneth S. Boling, B.S.

A Thesis

Approved by the Department of Geology

____
Stacy Atchley, Ph.D., Chairperson

Submitted to the Graduate Faculty of
Baylor University in Partial Fulfillment of the
Requirements for the Degree
of
Master of Science

Approved by the Thesis Committee

____
Stephen I. Dworkin, Ph.D., Chairperson

____
William C. Hockaday, Ph.D.

____
Robert R. Kane, Ph.D.

Accepted by the Graduate School
December 2013

____
J. Larry Lyon, Ph.D., Dean

Page bearing signatures is kept on file in the Graduate School.

TABLE OF CONTENTS

LIST OF FIGURES

LIST OF TABLES

ACKNOWLEDGMENTS

I would like to thank my advisor Dr. Steve Dworkin, my committee members Dr. Bill Hockaday and Dr. Bob Kane. I would also like to thank Dr. Ren Zhang and Dr. Don Parker for their assistance in laboratory analyses.

CHAPTER ONE

Introduction

Organic-rich mudrocks have long been recognized as a critical component of oil and gas exploration. Mudrocks with large amounts of organic matter are one of the most common source rocks for hydrocarbons, some of which may migrate to charge conventional plays in overlying sediments. Despite the relatively common occurrence of these formations, their fine-grained nature often limits their permeability, inhibiting the direct recovery of hydrocarbons using conventional means. Thus, organic-rich source rocks were not commonly exploited for oil and gas production. However, with the relatively recent technological advances made in the combined use of directional drilling and hydrofracturing, this type of formation has become a viable target for oil and gas production. As a result, these resource plays that have been termed "unconventional reservoirs" are now becoming more conventional.

One such organic-rich source rock which has gained significant attention from both industry and academia in the past few years is the Eagle Ford Formation.; an Upper Cretaceous marine mudrock which was deposited on the southeastern margin of the Western Interior Seaway (WIS) of North America (Arthur and Sageman, 2005; Donovan and Staerker, 2010). The Eagle Ford has been recognized as being the likely source rock for some of the conventional plays in the East Texas and Maverick basins (Surles, 1986; Magoon, 1987; Wescott and Hood, 1994). Despite the economic significance of the Eagle Ford, the processes responsible for the accumulation of large quantities of organic matter within this formation are still debated.

Sediments deposited under normal marine conditions, do not usually inherit high concentrations of organic matter because the majority of the net primary productivity generated by photosynthetic algae in the photic zone is rapidly decomposed and remineralized to CO_2 by heterotrophic organisms before it reaches the sea floor resulting in less than 10% of the total productivity being exported from the photic zone (Seibold and Berger, 1996). In addition, only a fraction of the deposited organic matter is preserved in sediments due to the additional remineralization of organic matter within shallowly buried sediments (Canfield, 1994). Therefore, the accumulation of substantial amounts of organic matter in marine sediments requires oceanographic conditions which favor either increased primary productivity or increased preservation of organic matter (Jenkyns, 2010).

The character of the Eagle Ford Formation is apparently the result of the global oceanic anoxic event OAE-2 which coincided with its deposition. Oceanic anoxic events represent periods during which low O_2 concentrations dominated the deep oceans on a global scale (Schlanger and Jenkyns, 1976). Portions of the Eagle Ford have been previously described as being deposited under low oxygen levels, although precise correlation with the anoxic event OAE-2 has not been accomplished (Dawson and Almon, 2010).

Recent Eagle Ford subsurface studies have utilized trace metal geochemical data (e.g.,Kearns, 2012; Ratcliffe et al., 2012; Moran, 2013) to gain insight into paleoceanographic conditions that existed during deposition. Outcrop studies, which have focused on lithology and biostratigraphy, have also been undertaken (Stephenson, 1929; Adkins and Lozo, 1951; Charvat, 1985; Jiang, 1989; Dawson, 1997, 2000). At least one outcrop study which focused on the organic geochemistry of the Eagle Ford has also been conducted (Liro et al., 1994). However, a study combining both organic and inorganic geochemistry has not been performed for the portions of the Eagle Ford that outcrop in central Texas.

Therefore, the goals of this study were to: 1.) assemble a composite section of the Eagle Ford from a series of outcrops in central Texas, 2.) document the chemostratigraphic character of this composite section using both organic and inorganic geochemistry, 3.) use the geochemical data to determine the evolution of the paleoceanographic conditions (redox and productivity) that existed during Eagle Ford deposition, and 4.) use this information to determine the controls on the accumulation of organic matter in the Eagle Ford.

The Geochemistry of Organic Rich Mudrocks

This section briefly summarizes the use of trace metal concentrations and organic matter geochemistry as indicators of paleoceanographic conditions. More detailed descriptions of these methods and their limitations can be found in ((Brumsack, 2006; Tribovillard et al., 2006) and the references therein.

The amount of organic matter that becomes preserved in sediments is largely controlled by three processes: 1.) the net primary productivity, 2.) the decomposition rate of the organic matter, and 3.) the rate of sedimentation (Pedersen and Calvert, 1990; Sageman et al., 2003). The sedimentation rate has the potential to affect organic matter abundance through the process of dilution as well as controlling the amount of time organic matter is exposed to oxygen (Hartnett et al., 1998). In modern depositional settings two processes result in high OC content: 1.) coastal upwelling that enhances nutrient delivery to the photic zones and 2.) the occurrence of anoxic seawater (Brumsack, 2006). High sedimentation rates enhance the preservation of OC for both of these situations, while low sedimentation rates result in the accumulation of organic matter only under anoxic conditions (Canfield, 1994). Geochemical attributes of the sediment and the organic matter lend insight into which process is controlling the accumulation of organic matter.

Paleo-redox conditions control the preservation of organic matter primarily because of the amount of dissolved oxygen in the seawater. Because of the kinetically rapid of oxygen as an electron acceptor by bacteria its presence facilitates the destruction of organic matter. In the absence of free O_2 , less efficient terminal electron acceptors are utilized during organic matter degradation. These alternative pathways used by bacteria during the decomposition of organic matter follow a prescribed order starting with denitrification, and then followed by manganese reduction, iron reduction, sulfate reduction, and finally methanogenesis (Froelich et al., 1979). In addition, trace elements with more than one common valence undergo a variety of dissolution, precipitation, and exchange reactions depending on the Eh of seawater. Thus, paleo-redox conditions may be determined by enrichments or depletions of these redox-sensitive trace elements (Brumsack, 2006; Tribovillard et al., 2006).

The terminology used to describe ecosystem oxygen level is defined by (Tyson and Pearson, 1991) and includes oxic, suboxic, anoxic, and euxinic conditions defined by the concentration of dissolved O_2. Oxic conditions are defined as being greater than 2.0 ml O_2/l H_2O, suboxic conditions occur between 2.0 and 0.2 ml O_2/l H_2O, and anoxic being less than 0.2 ml O_2/l H_2O. Euxinic conditions occur when oxygen levels are low enough that free H_2S is present in the water due to bacterial driven sulfate reduction, which can react with detrital Fe to form pyrite and other iron sulfides (Berner, 1982).

The trace elements most commonly used to interpret redox conditions are Mo, V, and U. These elements go into solution in under oxic conditions and precipitate under anoxic conditions (Tribovillard et al., 2006). In the case of Mo, enrichment in mudrocks is thought to occur only in the presence of free H_2S during euxinic conditions, which activates a "geochemical switch" through the formation of thiomolybdates which become particle reactive allowing adsorption to clays and organic matter (Helz et al., 1996).

Other elements also affected by redox conditions include Mn and Fe, which generally dissolve under anoxic conditions and precipitate under oxic conditions(Tribovillard et al., 2006). This can result in a phenomenon known as Fe-Mn cycling as these elements may precipitate in oxic waters and sink below the chemocline where they dissolve. Thus high concentrations of Fe and Mn may indicate deposition under oxic conditions. Conversely, under reducing conditions Fe may be sequestered into the sediment by the precipitation of pyrite and Mn precipitation under reducing conditions can occur as a carbonate (Calvert and Pedersen, 1993).

The accumulation of large amounts of organic matter may be also be controlled by high rates of productivity and is typically brought about by high nutrient availability with nitrogen, phosphorous or iron usually being the limiting nutrient. Nutrients are ultimately derived from the continents and are transported to the oceans through fluvial, groundwater or atmospheric processes. However, the most abundant source of nutrients in the marine environment is from the upwelling of deep seawater, a process that represent nutrient cycling from the bacterial decomposition of primary producers

(Sverdrup et al., 1942) (Piper and Calvert, 2009). Productivity is typically assessed by the abundance of the trace elements Cu, Zn, and Ni. These elements are considered to be bio-essential and are delivered to the sea floor bound in organic matter. Other productivity indicators include high levels of P, although anoxic conditions may cause P to dissolve resulting in diminished concentrations within the sediment.

Productivity and preservation rates directly affect each other. For example, when massive increases in oceanic productivity occur, the abundance of photoautotrophic algae overwhelm the available oxygen supply (Meyers et al., 2006). During these periods of accelerated algal growth the influx of organic matter depletes the available oxygen as algal decomposition proceeds resulting in anoxic conditions in the bottom waters. In addition, within the resulting anoxic bottom waters the biolimiting nutrient P goes in to solution and may be recirculated back into the photic zone resulting in a positive feedback between primary production and organic matter production (Van Cappellen and Ingall, 1994; Ingall and Jahnke, 1997)

Trace element concentrations can also be controlled by depositional processes and it is therefore important to identify which metals are useful for ocean-chemistry reconstruction. The trace elements which are deposited with detrital sediments may be differentiated from those that are precipitated under anoxic conditions by comparing them to Al, Ti, or Zr. These three elements are considered to be derived only from the detrital fraction and are usually immobile during diagenesis (Calvert and Pedersen, 1993). A positive co-variation of trace elements with Al, Ti, or Zr is indicative of the trace element being supplied by the detrital fraction.

Al is most commonly used for this kind of analysis because the Al content of a sediment is a good indicator of the clay content (Kryc et al., 2003). However, there are some circumstances in which Al is not appropriate as an indicator of the detrital fraction, such as when its concentration is lower than 3-5% (Murray and Leinen 1996). Additionally, the dilution effect may cause uncorrelated variables to appear correlated when normalized to Al (Van der Weijden, 2002). One approach to minimize normalization bias is to focus on the stratigraphic variation of Al normalized elements rather than using absolute values (Tribovillard et al., 2006).

In addition to normalization to Al, another commonly used technique for interpreting trace element data is to compare the composition of a mudrock sample to the "average shale" ((Wedepohl, 1971, 1991) by calculating the enrichment factor using the formula:

$$Enrichment\ Factor\ (EF) = \frac{(trace\ element/Al)_{sample}}{(trace\ element/Al)_{average\ shale}} \qquad \text{(Eq. 1)}$$

Using this method, elements which have an EF values greater than 1, are said to be enriched, while elements which have an EF of less than one are said to be depleted. This assessment has some drawbacks however, because the "average shale" value may not be universal due to differences in source material or diagenetic history (Van der Weijden, 2002).

For example, Mo occurs in the "average shale" at concentrations of around 1.3ppm (Wedepohl, 1971, 1991) but may become enriched to much higher concentrations in sediments deposited under low oxygen conditions. These properties make Mo and other trace elements that have been delivered to the sediment as a result of varying redox conditions useful for the interpretation of oxygen concentrations at the time of deposition.

Another useful proxy for redox conditions in mudrocks is the Th/U ratio. The similar valence and atomic radius of these two elements causes them to occur in proportional concentrations in crustal material (Adams and Weaver, 1958). Under anoxic conditions however, the precipitation of hydrogeneous U causes an increase in the proportion of U relative to the concentration of insoluble Th, causing a decrease in the ratio of Th/U. This ratio is a useful proxy for marine oxygen levels (Adams and Weaver, 1958) and is an independent and complimentary check from the enrichment factor method.

CHAPTER TWO

Geologic Setting

The Eagle Ford Formation outcrops along a northeast-southwest trend, spanning from Oklahoma down to southwestern Texas (Figure 2.1). The unit dips at about one degree to the southeast. The thickness of the Eagle Ford varies regionally and it is about 200ft thick in the Waco area but thins to the southwest toward Austin(Jiang, 1989).

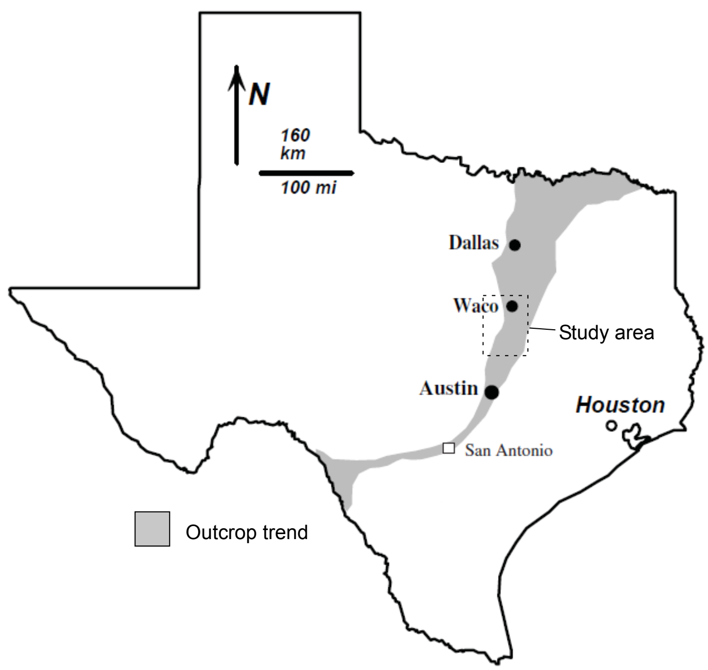

Figure 2.1. Outcrop trend of the Eagle Ford throughout central Texas. Modified from (Dawson, 2000).

The deposition of the Eagle Ford Formation occurred during the Late Cenomanian and Turonian stages of the Late Cretaceous. During this time, a generally warm climate with relatively high atmospheric pCO_2 levels dominated (Veizer et al., 2000; Bice et al., 2006). Global eustatic sea level reached the Cretaceous maximum following a prolonged rise in sea level (Haq et al., 1987) and the poles were ice free.

The Eagle Ford was deposited over a wide area comprising inner to outer shelf environments on the southern margin of the Western Interior Seaway (Surles, 1987) (Figure 2.2).

Figure 2.2. Paleogeographic reconstruction of North America during the Late Cretaceous. Extent of Eagle Ford deposition is shown. Modified from (Blakey, 1994).

The regional lithostratigraphy of the Eagle Ford is complex and varies regionally due to the uplift of the San Marcos arch, the Sabine uplift, and the proximity to the shore line. In the study area of north-central Texas, the Eagle Ford unconformably overlies the Woodbine Formation and unconformably underlies the Austin Chalk (Figure 2.3). In southwestern Texas the Eagle Ford unconformably overlies the Buda Formation (Martin et al., 2011). The San Marcos arch, a topographic high that existed during deposition, separated the East Texas Basin along with the area investigated in this study from the Maverick Basin to the southwest (Hentz and Ruppel, 2010) (Figure 2.3).

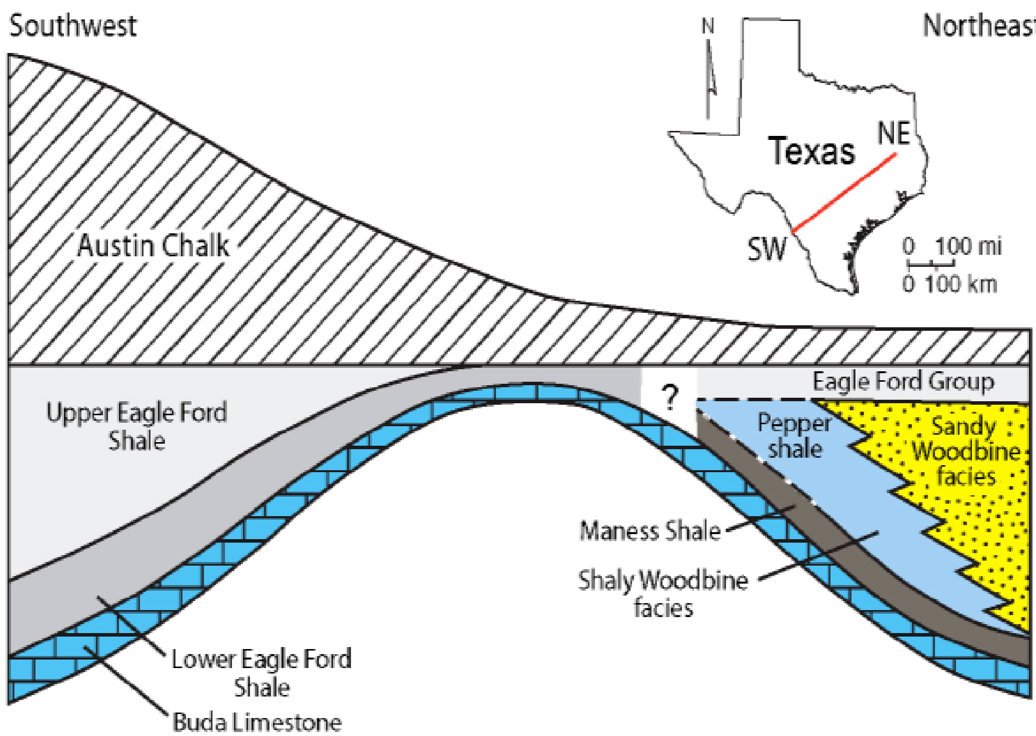

Figure 2.3. Regional stratigraphic variations associated with the Eagle Ford are most pronounced on each side of the San Marcos Arch . From (Hentz and Ruppel, 2010).

In the study area, the Eagle Ford has been divided into three members, the Lake Waco, South Bosque, and Arcadia Park (Jiang, 1989). The boundary between the South Bosque and Lake Waco members encompasses the Cenomanian/Turonian (92 ma) boundary. This boundary marks the occurrence of the well documented Oceanic Anoxic Event OAE-2 (Schlanger and Jenkyns, 1976). The deposition of the Eagle Ford coincides with a transgression and high stand which may also have been responsible for the production of several other worldwide organic rich mudrocks (Liro et al., 1994; Dawson, 2000).

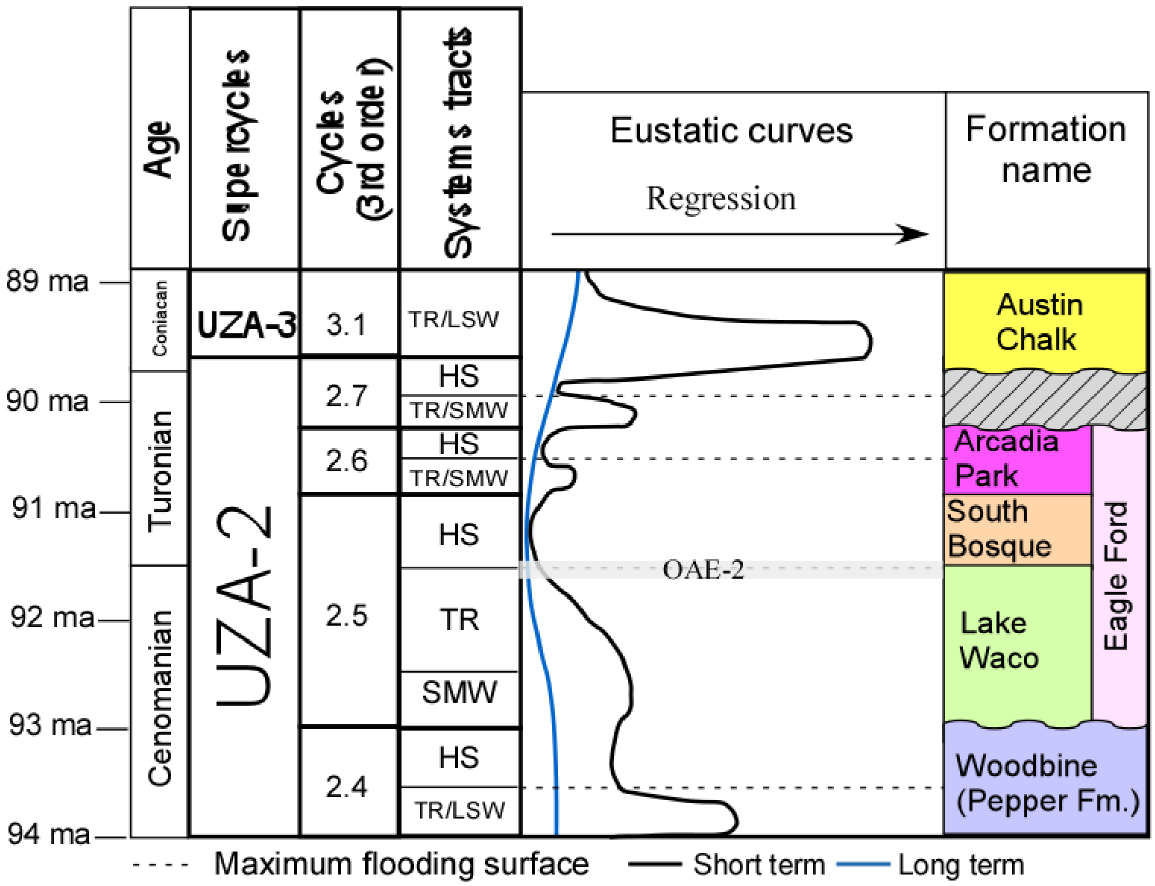

Figure 2.4. Eustatic sea level through the Late Cretaceous and stratigraphy of the Eagle Ford for Central Texas. Adapted from (Haq et al., 1987; Jiang, 1989; Liro et al., 1994)

The Eagle Ford is typically divided into two sub-formations based on lithology; the lower Lake Waco member, and the upper South Bosque member. The Lake Waco member is generally more carbonate rich than the South Bosque and contains many bentonite seams. This member typically consists of dark, silty shale with interspersed laterally discontinuous carbonate layers. In addition to limestones and shales, bentonites are also common throughout the Lake Waco. These bentonites are thought to be formed from volcanic ash falls sourced from several vents located in southern Arkansas and on the Monroe uplift (Hunter and Davies, 1979; Byerly, 1991). The upper South Bosque Formation contains fewer bentonites.

The Eagle Ford is overlain by the Austin Chalk in both the northeast and southwest. The Austin Chalk consists of interbedded chalks, volcanic ash, and marls (Martin et al., 2011). The contact between the Austin chalk and the Eagle Ford has been described as unconformable in central Texas (Stephenson, 1929; Jiang, 1989). However, this contact is said to be conformable in outcrop in west Texas (Freeman, 1961; Lock and Peschier, 2006) and there may be additional units between the Eagle Ford and Austin Chalk in this region (Donovan and Staerker, 2010). The Austin Chalk- Eagle Ford contact marks the Turonian/Coniacian boundary at (89 ma) that represents a major unconformity (Stephenson, 1929).

The Woodbine/Pepper Formation was deposited during the high stand following the Middle Cretaceous Unconformity marking the shift from carbonate dominated shelf to clastic deltaic and coastal depositional systems (Galloway, 2008). In the study area the pepper shale was part of a distal prodelta that was sourced from the prograding Woodbine delta to the southwest into the East Texas basin (Oliver, 1971; Turner and Conger,1984). The uplift of the Sabine arch effectively separated the Woodbine delta from the Tuscaloosa delta to the east (Figure 2.4). Following the deposition of the Pepper shale erosion and truncation of this unit occurred in the East Texas basin due to the continued uplift and subaerial erosion of the Sabine arch (Galloway, 2008). This was then followed by a sea level rise, the onset of lower Eagle Ford deposition as well as the renewed progradation of the Tuscaloosa delta (Figure 2.5). During the ensuing high stand the upper Eagle Ford (South Bosque member) was deposited (Jiang, 1989). The separation of the Woodbine and Tuscaloosa deltas by the persistently high Sabine arch effectively created two concurrent depocenters within the Gulf of Mexico basin. Woodbine sediments have been described as being sourced from the Ouachita and Arbuckle Mountains (Stehli et al., 1972) whereas the Tuscaloosa sediments were sourced from the stable craton.

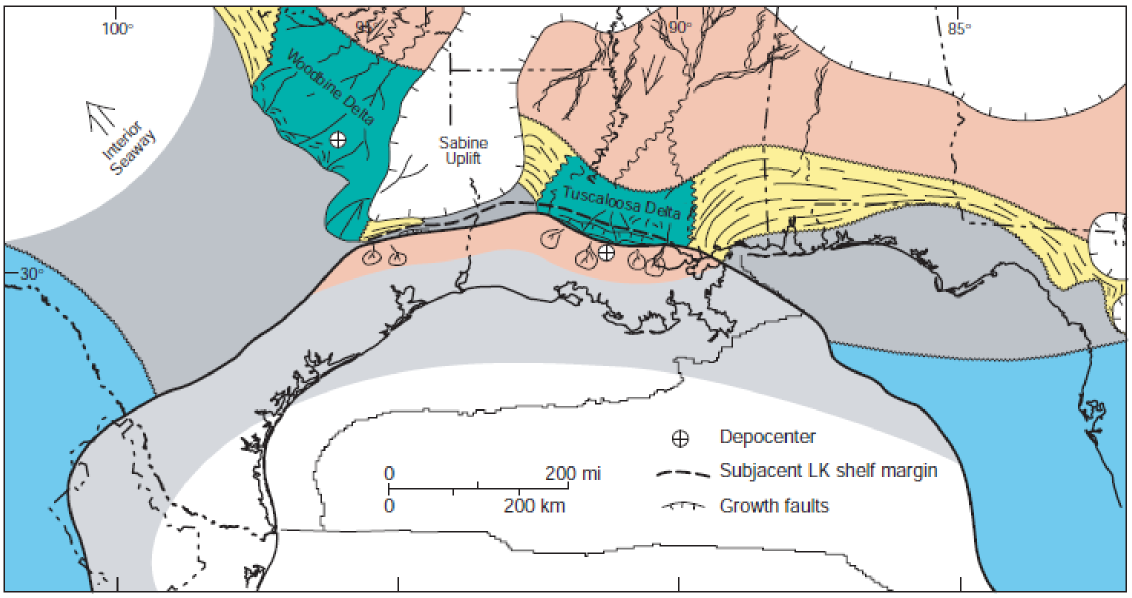

Figure 2.5. Depositional setting of the Gulf of Mexico showing sources of clastic material during the Late Cretaceous. Ongoing uplift of the Sabine arch separated the two clastic depocenters and dispersal systems.(Galloway, 2008).

CHAPTER THREE

Methods

The outcrops of the Eagle Ford which were selected for this study are all within McClennan County. The advantage of an outcrop study is being able to see the lateral extent of some features which may be discontinuous on the scale of core. The Eagle Ford in central Texas occurs as small exposures that are scattered across a large area. The lack of good exposures is due to the poor cohesive strength of the rocks (Hsu and Nelson, 2002). Consequently, one of the early challenges of this project was to determine the stratigraphic relationship between these small geographically far spaced outcrops. Relative stratigraphic position was determined using geologic maps, outcrop descriptions from other surveys, the general strike and dip of the rocks, and chemostratigraphy.

The majority of the outcrops sampled were located using information from previous studies of the Eagle Ford (Charvat, 1985; Surles, 1986; Jiang, 1989; Liro et al., 1994). Several of the smaller outcrops reported in older publications, especially those which did not occur along active streams, have been heavily eroded and are no longer accessible and thus an effort was made to locate new unstudied outcrops. One method for locating previously unreported outcrops was to use the available Texas State topographic maps in a GIS database to generate a map that could be used to identify areas displaying rapid changes in elevation and high slope angles where outcrops were likely to form. This information was then combined with the Texas state geologic map as an overlay which revealed the locations of potential outcrops. Using this method, a relatively large, previously unreported outcrop of the Lake Waco Fm. (outcrop HD) was discovered along a creek that drains into Lake Waco. The primary limitation of using the GIS database is the low resolution of the available topographic data set.

Each outcrop was described and measured using a Jacob staff. Approximately 30-50g of rock was collected at ~20cm intervals. Unweathered samples were obtained by digging trenches 20-50cm back into the outcrop. Fresh samples were identified on the basis of a lack of iron staining, absence of gypsum crystals and fine roots, as well as the presence of unweathered pyrite. A total of 166 samples were collected from nine outcrops and these samples were stored in plastic bags to await processing and analysis.

Organic Matter Analysis

The abundance and character of organic matter in each sample was determined. This analysis includes the wt.% TOC, wt.% N, $\delta^{13}C_{org}$, and δ^{15}Norg. Samples were pretreated with 10% HCl in silver cups before combustion in a Costech elemental analyzer. The evolved C and N gases were then conveyed to a Thermo Scientific™ Delta V Advantage stable isotope mass spectrometer for C and N isotope ratio determination. The analytical precision for concentration analysis is +/- 0.08 for carbon and +/- 0.01for N. Precision for isotopic analysis is +/- 0.03 for $\delta^{13}C$ and +/-0.06 for $\delta^{15}N$.

Elemental Analysis

The elemental concentrations for 10 major elements (SiO_2, TiO_2, Al_2O_3, Fe_2O_3, MnO, MgO, CaO, Na_2O, K_2O, P_2O_5) and 18 trace elements (As, Ba, Co, Cr, Cu, Mo, Nb, Ni, Pb, Rb, Sc, Sr, Th, U, V, Y, Zn, and Zr) were determined for each sample. The major elements are reported as wt. % oxides and trace elements are reported in ppm.

Elemental concentrations were determined for each sample using a Rigaku ZSX-Primus 2 Wavelength Dispersive X-Ray Fluoresce spectrometer (WD-XRF) using a 4.0kW Rhodium target X-ray tube. Each sample was prepared for XRF analysis using the following procedure. Field samples were placed into a drying oven set at 40° C for 48 hours. Samples were then powdered using a tungsten carbide shatter-box, which was cleaned thoroughly with acetone between each sample to prevent cross contamination. In addition, a "pre-contamination" treatment was performed by grinding a small amount of the sample and then cleaning again with acetone. The actual sample was then placed in the shatter-box and pulverized for two minutes. Crushed samples were stored in plastic vials. Six grams of this powdered sample was mixed with 1.00g of cellulose binder, and this mixture was placed inside an aluminum cup and pressed into a solid pellet using a hydraulic press. The completed pellets were then stored in small plastic boxes to prevent dust from contacting the sample.

Due to the nature of the mixed siliciclastic and carbonate composition of the Eagle Ford the calibration of the XRF was performed using a combination of in house and internationally accepted standards for shales and carbonates.

CHAPTER FOUR

Results

The composite section is constructed from 9 outcrops located around McLennan County (Figure 4.1). Detailed stratigraphic columns and descriptions of these outcrops can be found in appendix A. A total of 166 samples were collected from these outcrops and these samples were analyzed for total organic carbon (TOC), total nitrogen (TON), $\delta^{13}C_{organic}$, $\delta^{15}N_{organic}$, as well as elemental concentrations for 28 elements. These geochemical data are presented in appendix B.

Composite Section

The outcrops were placed in stratigraphic order to construct the composite section presented in Figure 4.2. This composite section shows the general succession of lithologies within the Pepper shale and Eagle Ford Formation. After comparison of the geochemical data (Figure 4.3) and the pattern and thickness of bentonite beds, it was determined that outcrop WPDS duplicates part of the section contained within outcrop HD. This illustrates the utility of the geochemical data for correlation purposes and suggests that this technique will have application for subsurface correlations using well log data.

The lithologies of the Eagle Ford and Pepper Formations differ significantly (Figure 4.2). The Pepper Formation is a black, non-calcareous, claystone with thin sandy intervals. The contact between the Pepper and the Eagle Ford is disconformable. The lower Eagle Ford (Lake Waco member) is coarser grained than the Pepper and contains

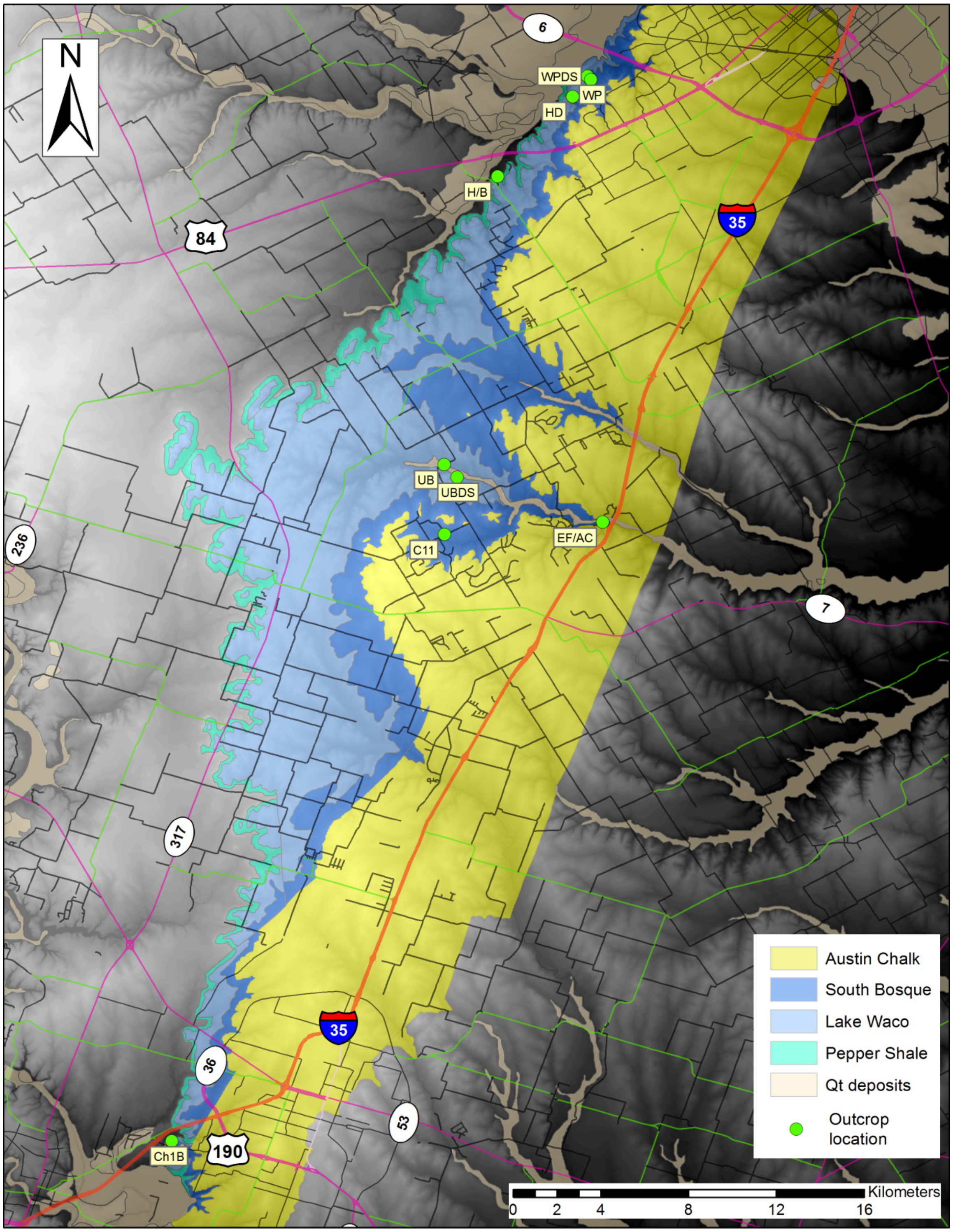

Figure 4.1. Outcrop locations in the Waco area. Compiled from the Texas state geologic map and topographic maps. Road data obtained from the Texas DOT roadways 2012 map.

abundant calcite mud. Additionally, interbedded limestones within the Lake Waco member occur as discontinuous beds or small lenses composed of coarse shell fragments and thin bentonites beds are common.

The upper Eagle Ford (South Bosque member) is characterized by abundant calcite in its lower portion which steadily declines up section. At the top of the South Bosque the mudrock becomes calcite free and this calcite-free mudrock has been named the Arcadia Park member by ((Jiang, 1989).

The composite section is comprised of six chemofacies (A-F) that were identified based on changes in mudrock geochemistry. Chemofacies A is the Pepper Formation, which is identified by higher concentrations of the major elements Al, Si, K, Ti (all being controlled by the relative abundance of detrital minerals) and lower Ca concentrations than the overlying Eagle Ford (Figure 4.4). Chemofacies B is identified by higher Fe and P than the rocks above and below it, as well as distinctive C/N ratios. Chemofacies C is defined by lower Fe and P than chemofacies B (Figure 4.4). Chemofacies D is defined by an abrupt change in major and trace elements as well as a positive carbon isotope excursion. Chemofacies E is characterized by a low concentration of redox-sensitive trace elements and chemofacies F is defined by high concentrations of Al, Si, K, Ti and low Ca.

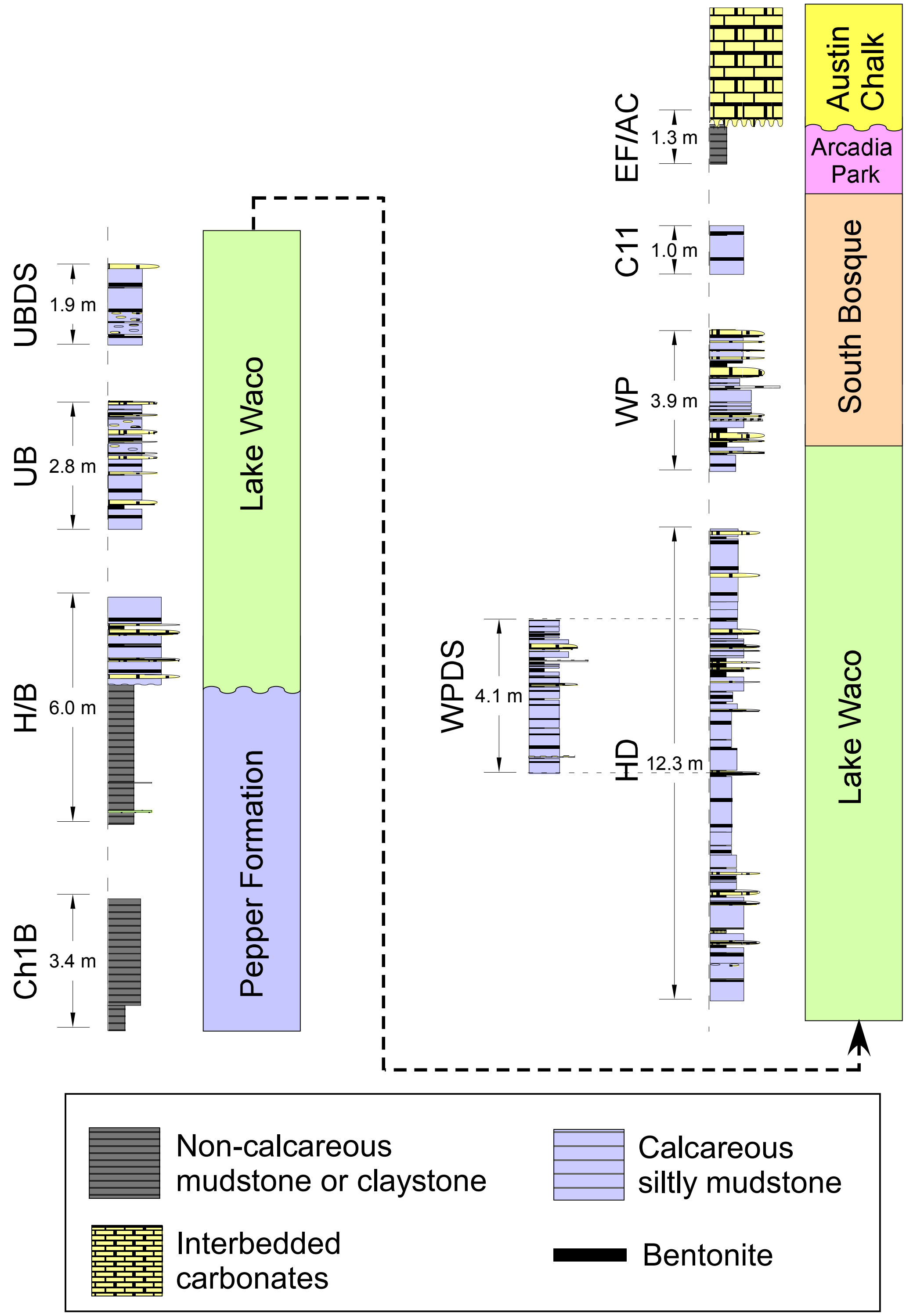

Figure 4.2. A composite stratigraphic section of the Pepper and Eagle Ford Formations in central Texas. The amount of section between outcrops is unknown and therefore the gaps are not to scale.

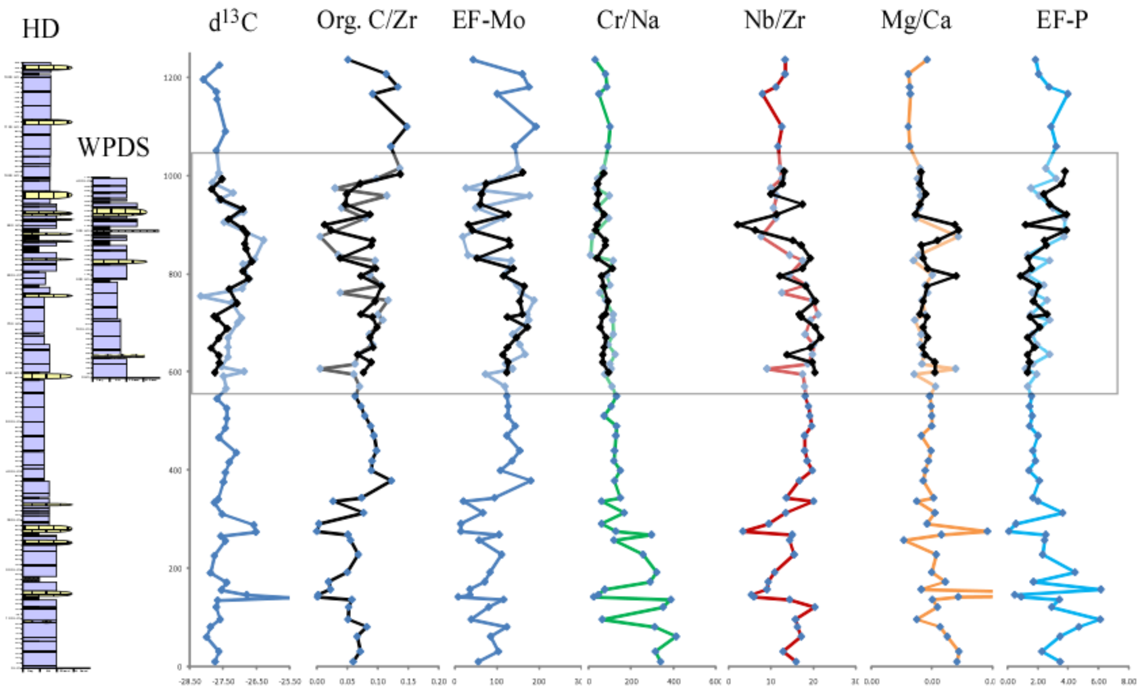

Figure 4.3. Based on stratigraphic patterns (left two columns) and various geochemical data, the stratigraphic interval in outcrop WPDS appears to be encompassed within the thicker HD outcrop. Geochemical data presented with black lines are data from outcrop WPDS.

Major Elements

The major element concentrations of the Eagle Ford reflect the varying abundance of the different minerals comprising the mudrock. The mineral proportions of the Eagle Ford are highly variable depending on inputs from detrital and biogenic sediment sources. Most of the chemostratigraphic facies can be identified by major element chemistry which are shown in Figure 4.4.

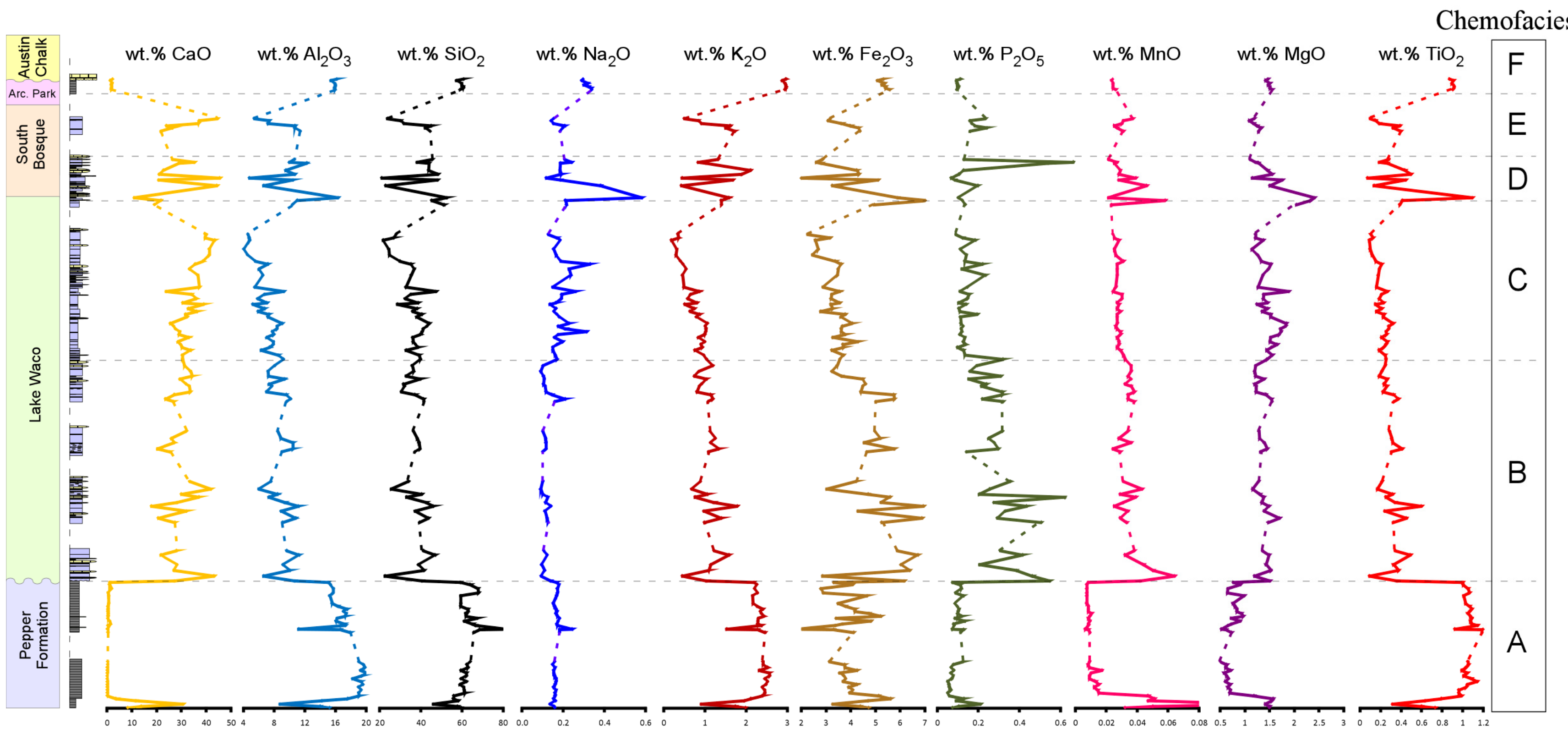

Figure 4.4. Stratigraphic pattern of major elements within the Pepper and Eagle Formations in central Texas. Chemostratigraphic facies designations are shown in the far right column. The most significant changes in major element concentrations occur at the transition from chemofaceis A to B and E to F due to the presence or absence of calcite.

Differences in major element concentrations are noted to occur at the contact of the Pepper Formation and the Eagle Ford, designated in Figure 4.4 as the transition from chemofacies A to B. The transition is marked by an abrupt change in the concentrations of all the major elements. This reflects the change in lithology between the calcareous shale of the Eagle Ford and the non-calcareous Pepper Formation (Figure 4.2). The presence of calcite results in increased Ca and Mg concentrations while Al, Si, Na, K, and Ti concentrations fall as the abundance of clay minerals is diluted by the biogenic calcite. In contrast, the redox sensitive elements Fe and Mn, and the bioessential element P increase in chemofacies B due to lower Eh and higher productivity conditions associated with Eagle Ford deposition. Continuing up section, the Lake Waco member exhibits a gradual decline in Al, K, and Si as Ca and Mg concentrations continue to increase through chemofacies B and C reflecting increasing calcite abundance. Within the Lake Waco member the transition from chemofacies B to C was identified by a sudden decline in Fe, P and Mn. This transition occurs about one third of the way through outcrop HD and corresponds to a change in grain size from a silty mudstone to a finer-grained mudstone and the disappearance of the interbedded carbonate lenses seen in chemofacies B (see Figure A.6 in appendix A). The B/C chemofacies transition also corresponds to a slight increase in Na.

The beginning of chemofacies D corresponds to the base of the South Bosque member and is identified by sudden and large changes in major element concentrations compared to the underlying rocks. At the base of chemofacies D, the elements Na, K, Fe, Mn, Mg, Ti, and Al all display increases in concentration. In the small section of the South Bosque (outcrop C11) which was sampled, the elements K, Al, Si, and Ti are highly correlated to the amount of Ca and are controlled by the dilution of detrital sediments by calcite,.

Finally, the top of the Eagle Ford (Arcadia Park member, chemofacies F) is distinctive because of the sudden lithologic change to a calcite-free mudrock which is reflected by higher concentrations of Ti, Al, Si, and K and a dramatic reduction in the concentration of Ca from the underlying chemofacies E.

Trace Elements

In order to differentiate between trace metals bound within the detrital fraction from those whose concentrations are controlled absorption or precipitation caused by redox conditions, cross plots were constructed of trace metals versus aluminum (Figures 4.5 and 4.6). Well defined positive correlations between trace metals and aluminum concentrations (titanium and zirconium work equally well) indicate that the element is associated with the detrital fraction (Tribovillard et al., 2008). Although this group of trace elements cannot be used for the interpretation of anoxia or productivity, they may be useful for gaining insight into changes in sediment provenance or hydrologic regimes(Ratcliffe et al., 2010, 2012).

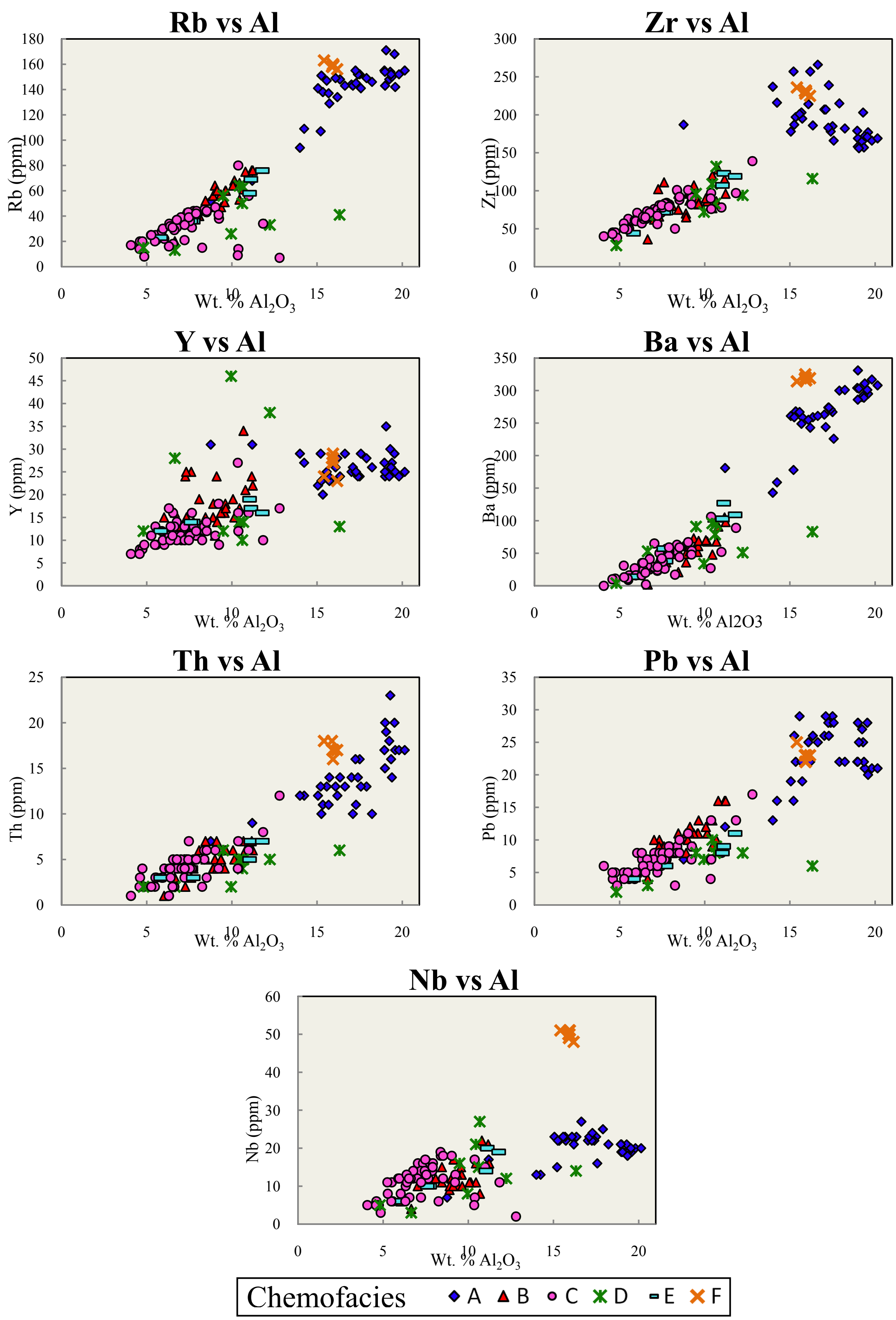

Figure 4.5. Trace elements that display a strong positive co-variation with aluminum. The concentration of these elements is controlled by the abundance of the detrital sediment. The legend shows the symbols for each chemofacies.

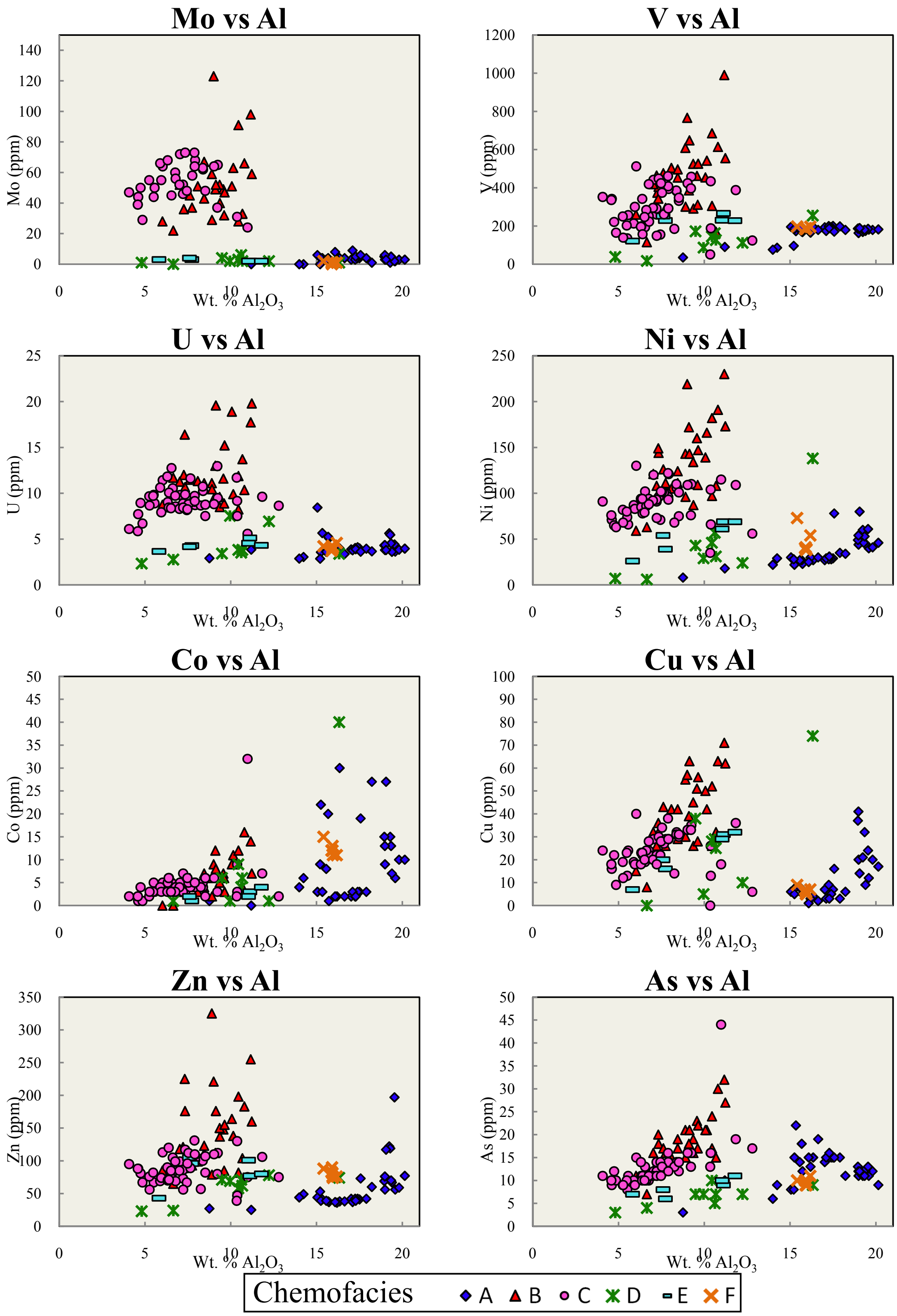

Figure 4.6. Trace elements that that lack strong positive correlations with aluminum. The concentration of these elements is more likely to be controlled by absorption or precipitation due to redox conditions or they may be bioessential nutrients bound up in organic matter. The legend shows the symbol for each chemofacies.

The cross plots in Figure 4.5 and 4.6 indicate that the trace elements Rb, Zr, Y, Ba, Th, Pb, and Nb correlate well with Al and therefore appear to be associated with the detrital fraction. In contrast, the elements As, Mo, Ni, V, Cu, Co, U, and Zn are poorly correlated with Al (Figure 4.6) indicating that the control on their concentration is not related to the abundance of detrital fraction minerals. The elements Mo, V, U, Cu, Ni, and Zn are all commonly used as proxies for redox conditions and biological productivity and their lack of correlation with Al in the Eagle Ford suggests that they are appropriate for paleoceanographic reconstruction.

The trace metals that are bound in the detrital fraction can be used to identify changes in sediment provenance. This is accomplished through a comparison between Nb and Ti because changing ratios between these two immobile elements are indicative of different source rocks (Ratcliffe et al., 2012). The relationship between these two elements is presented in Figure 4.7 which shows that the clastics making up the Pepper Formation (chemofacies A) have a different Nb/Ti ratio than those of the overlying Eagle Ford suggesting a different provenance. Furthermore, similar Nb/Ti ratios for the entire Eagle Ford suggests an unchanging provenance during its deposition.

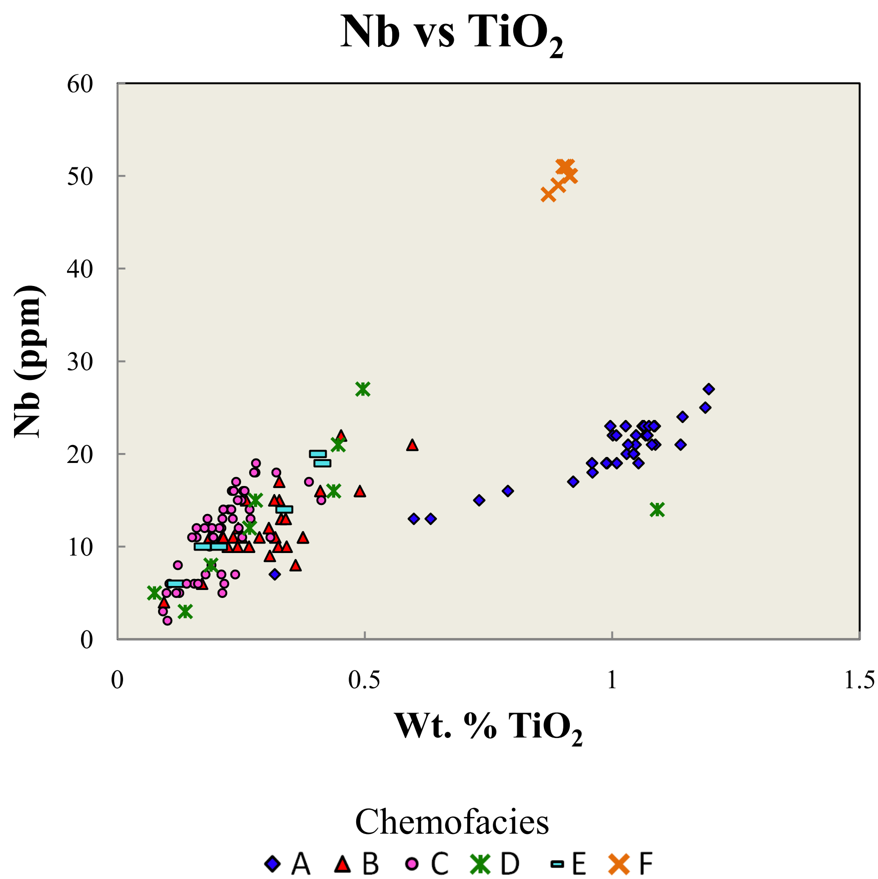

Figure 4.7. Nb vs. Ti for all of the mudrocks in this study. The Pepper shale samples fall off the trend identified by the Eagle Ford indicating a difference in source material (Ratcliffe et al., 2012). Legend shows the symbols used for the different chemofacies.

Because the trace elements traditionally used to evaluate productivity (Zn, Ni, Cu) and redox conditions (Mo, V, U) have been identified as having a non-detrital origin, they will be used to interpret paleoceanographic conditions during Eagle Ford deposition. The significance of these trace metal is investigated by calculating their level of enrichment relative to the average shale (Equation 1). Enrichment factors for redox-sensitive elements are shown stratigraphically in Figure 4.8 and for productivity-sensitive elements in Figure 4.9. These figures illustrate that the Pepper Formation (chemofacies A) has normal concentrations of redox sensitive trace metals and is somewhat depleted in metals indicative of productivity. These metal concentrations contrast strongly with those in the overlying Lake Waco member (chemofacies B and C) which is marked by highly enriched concentrations of Mo, V, and U. The enrichment pattern of these trace metals are strongly correlated with each other suggesting that they are responding similarly to paleo-ocean chemistry.

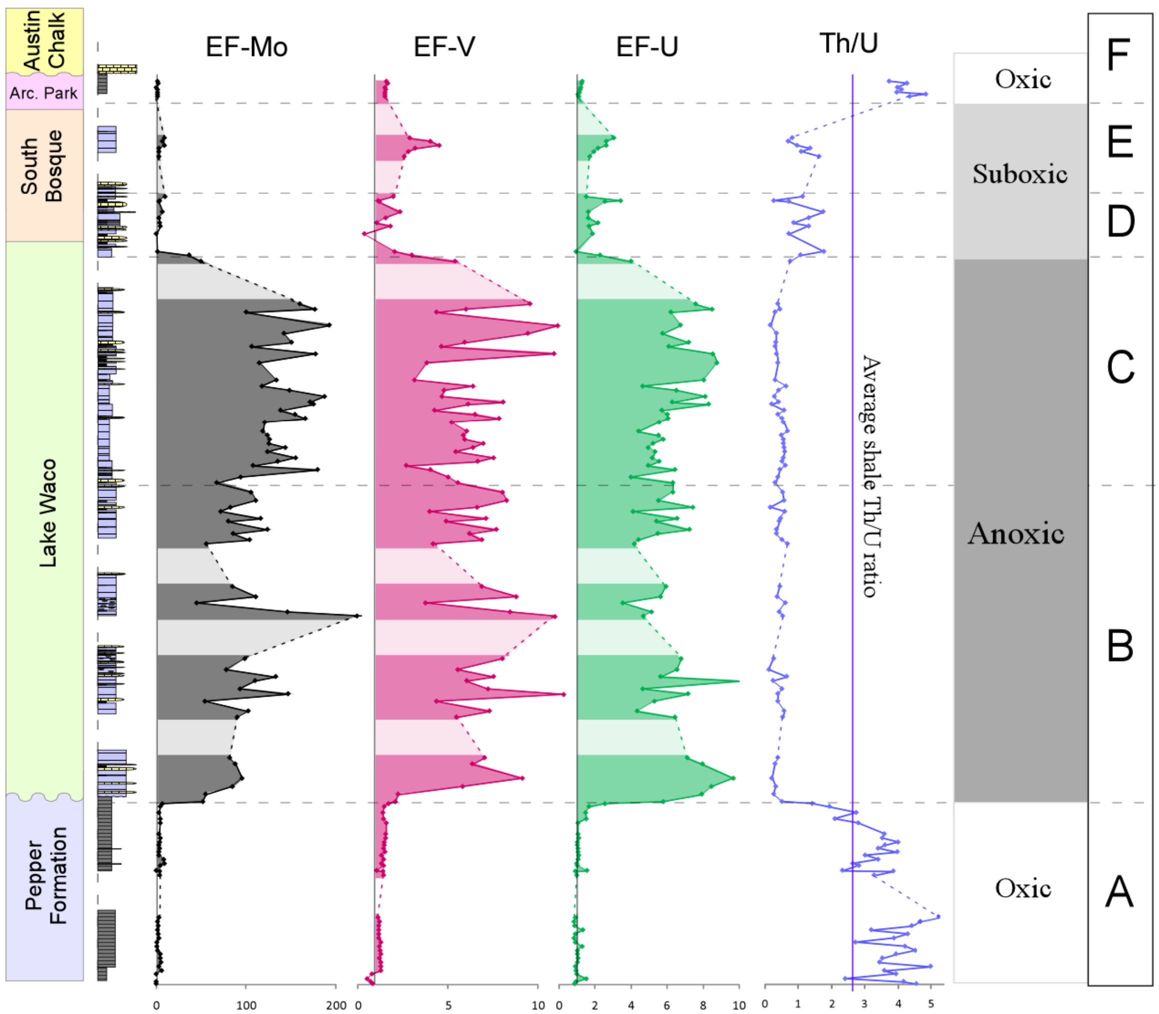

Figure 4.8. Enrichment factors for redox-sensitive elements, the gray lines indicate a ratio of 1.0. A value greater than 1.0 is considered to be enriched relative to the average shale (Wedepohl, 1971, 1991). Light colored bands represent the breaks between outcrops and are not to scale.

Paleoproductivity is best estimated using elemental species that are delivered to the sediments bound in organic matter. Ni, Cu, and Zn are important bio-essential trace elements that can be used for this purpose. The enrichments in these elements shown in Figure 4.9 may indicate that productivity was high for chemofacies B and C although considerable stratigraphic variability exists. The overlying South Bosque and Arcadia Park members (chemofacies D,E, and F) can be distinguished from the Lake Waco member by their much lower enrichments in both redox sensitive and productivity related trace metals (Figure 4.8 and 4.9).

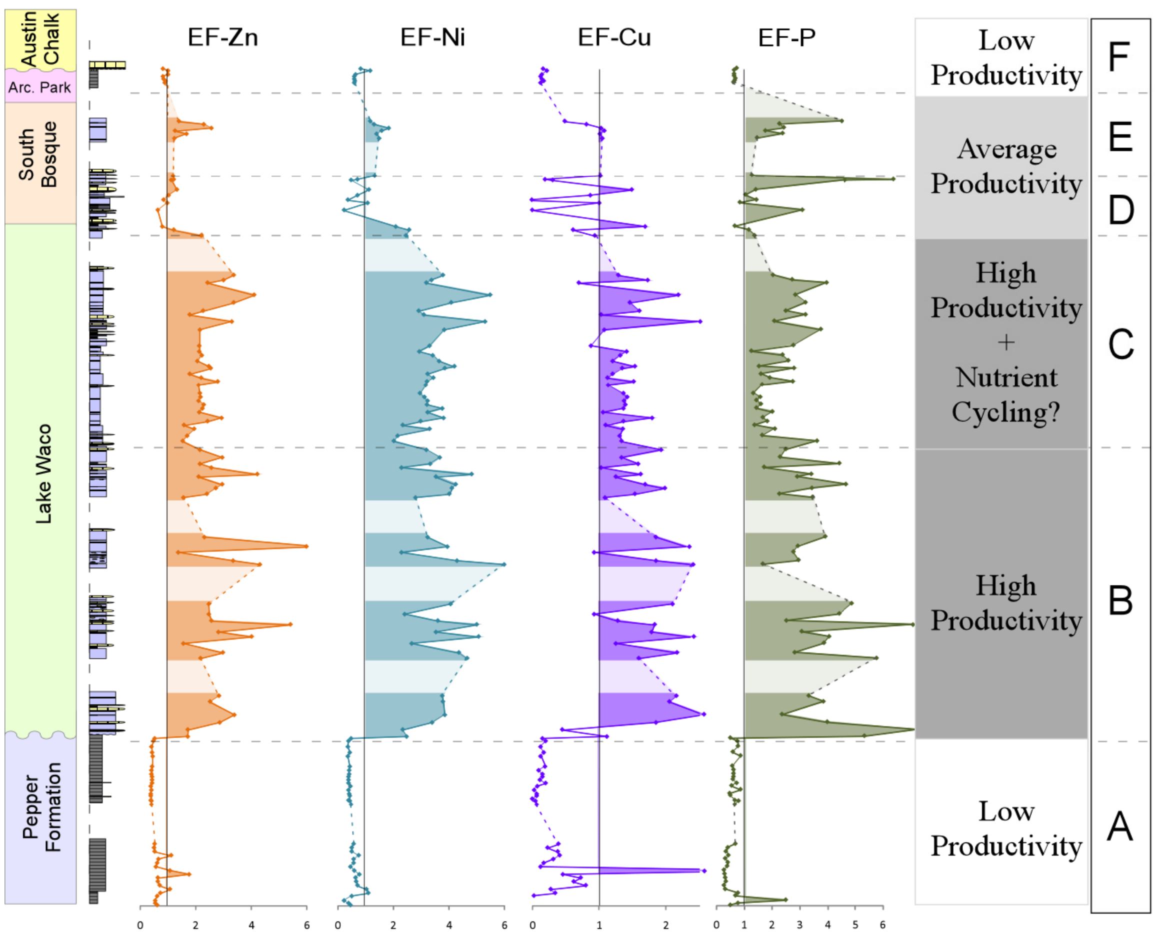

Figure 4.9. Enrichment factors for elements indicative of productivity. A value greater than 1.0 is considered to be enriched relative to the average shale (Wedepohl, 1971, 1991). Light colored bands represent the breaks between outcrops and are not to scale.

Organic Matter

The abundance and character of the organic matter in the Eagle Ford and Pepper Formation is quite different. The Pepper Formation (chemofacies A) has a relatively low TOC content, ranging from 0.26 to 2.00% with an average of 1.21%. The TOC content increases immediately at the base of the Eagle Ford (chemofacies B) to concentration of about 4% followed by an increase throughout the rest of chemofacies B that averages 6.07% (Figure 4.10). The highest measured organic carbon content (9.49%) occurs within this interval. TOC concentrations maintain their high concentrations through chemofacies C until a sudden decline at the onset of chemofacies D, followed by a slight recovery in chemofacies E, and then a decline to less than 1% in chemofacies F (Arcadia Park member). Total nitrogen concentrations are closely correlated with TOC indicating that nitrogen is organically bound. Although it is apparent that the fine grained mudrock samples of the Eagle Ford Formation have a high TOC content, the discontinuous and interbedded limestone layers have relatively little organic carbon by comparison.

The average $\delta^{13}C$ value of the organic carbon is fairly constant through most of the section at around -27‰ (VPDB). These delta values are considerably smaller than those found in modern marine organic matter, however they are typical for Cretaceous marine organic matter and have been attributed to high atmospheric pCO_2. There are three notable carbon isotope excursions present in the composite section. A 1‰ positive isotope excursion occurs at the contact between the Pepper shale and Eagle Ford and this carbon isotope shift is also accompanied by a decline in $\delta^{15}N$ (Figure 4.10). Another 1‰ positive excursion occurs further up the section in the middle of chemofacies C. This isotope excursion was identified in both the HD and WPDS outcrops (which stratigraphically overlap each other) and appears to coincide with an increase in the thickness and prevalence of bentonites and limestones. The most dramatic carbon isotope excursion occurs within chemofacies D and consists of 3‰ positive change. Chemofacies D is also characterized by a drop in TOC and total nitrogen concentration, as well as a shift to more negative $\delta^{15}N$ values (Figure 4.10).

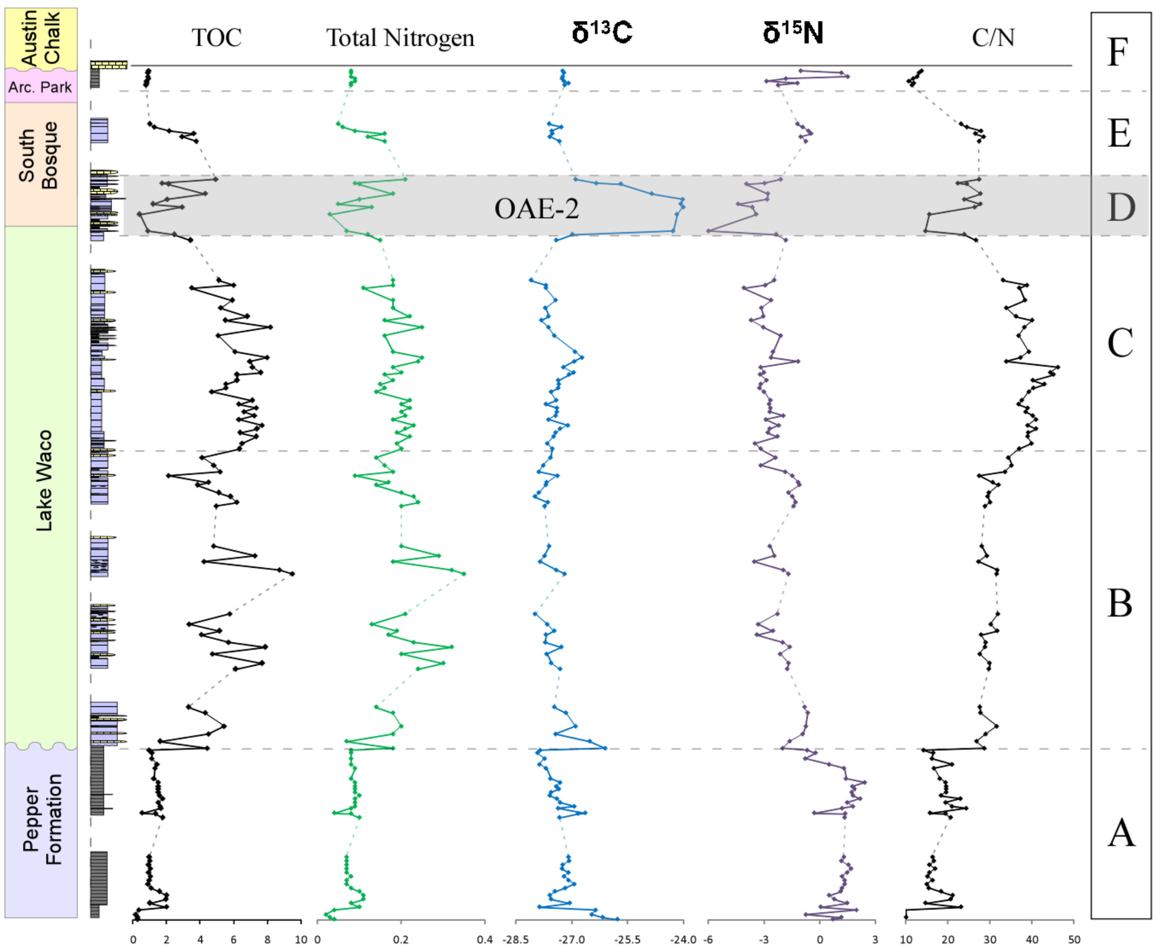

Figure 4.101. Total organic carbon, total nitrogen, $\delta^{15}N$, $\delta^{13}C$, and atomic C/N ratios for the composite section of Pepper and Eagle Ford outcrops. Note that the gaps between outcrops are not to scale.

The last attribute of the organic matter that was investigated is the stoichiometry of the organic matter. The molar C/N ratio for the Pepper Fm. (chemofacies A) averages around 17 while at the base of the overlying Eagle Ford the values increase to about 30 and then slowly continue to increase throughout the rest of chemofacies B. The organic matter in chemofacies C has the highest C/N ratios averaging slightly less than 40. C/N ratios decline at the top of chemofacies C and then maintain lower values in chemofacies D and E before returning to the levels similar to the Pepper Formation in chemofacies F.

A comparison of concentrations of redox sensitive and productivity-indicating elements against TOC reveals a strong correlation when TOC concentrations are higher than 2 wt. % (Figure 4.11). These cross plots show positive correlations between TOC and trace elements used for both redox and productivity proxies, however, it can be observed that chemofacies B and C have differing ratios.

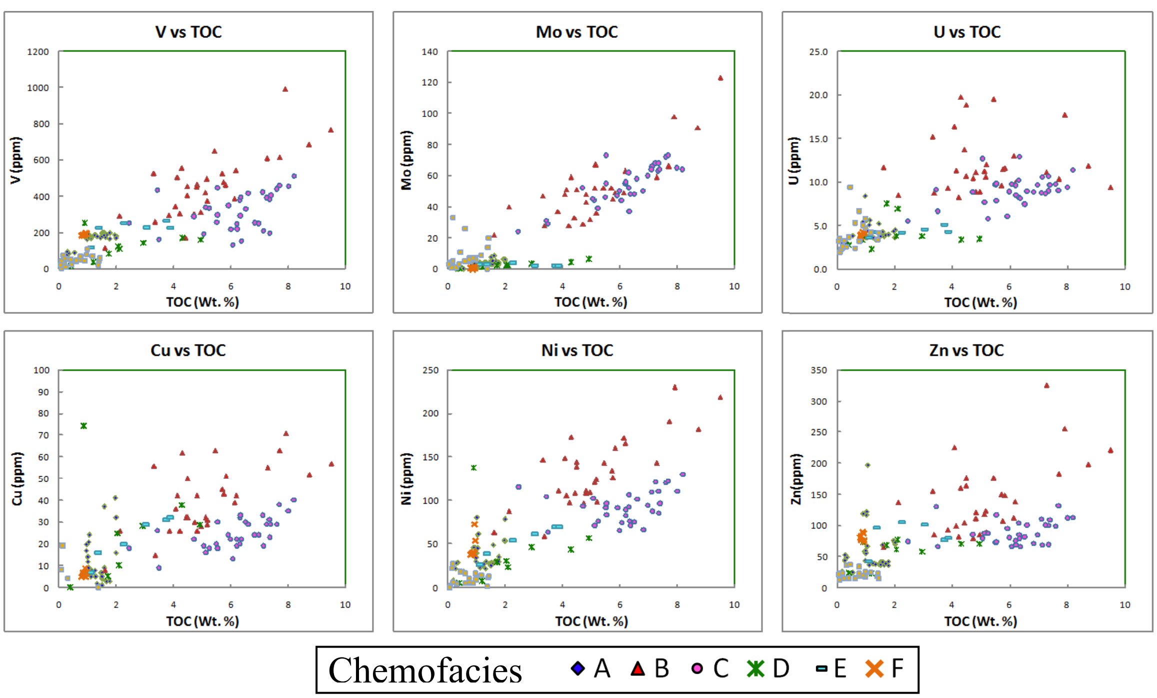

Figure 4.11. Trace element concentrations compared to TOC. Legend shows symbols used for the different chemofacies.

CHAPTER FIVE

Discussion and Synthesis

Chemofacies A

The low TOC exhibited by chemofacies A (Pepper Formation) along with the lack of enrichment of redox-sensitive and bio-essential trace elements, indicate that this formation was deposited under oxic conditions with low oceanic productivity (Figures 4.8 and 4.9). The very fine grain size and lack of carbonates corroborates a distal, prodelta depositional setting as has been suggested by (Galloway, 2008). Based on the Nb/Ti ratio, the source area for the clastic material of the Pepper Formation appears to have been different than that of the Eagle Ford.

Chemofacies B

Chemofacies B is the lower portion of the Eagle Ford Formation. Based on enrichments in the redox-sensitive trace elements Mo, U, and V it appears that the water column was anoxic during the entire deposition of this chemofacies. Mo enrichment is indicative of the presence of free H_2S suggesting that the bacterial degradation of organic matter was following the sulfate reduction pathway. Enrichments in Cu, Zn, and Ni indicate that productivity was high during this time while enrichments in P probably indicate higher nutrient availability. High oceanic productivity was most likely was the result of nutrient input from upwelling of deep nutrient-rich waters. The good correlation between the TOC and the redox-sensitive and bioessential trace elements for this chemofacies illustrates the ocean-chemistry control on organic matter accumulation.

The dominant control on organic matter accumulation in this interval seems to be high productivity which produced low oxygen levels as a result of organic matter decomposition depleting available oxygen.

Chemofacies C

The transition from chemofacies B to C is marked by a decrease in P, Mn, and Fe, and an increase in the enrichment of Mo, a shift to more negative $\delta^{15}N$ values, an increase in the molar C/N ratio, and most significantly, an increase in TOC. The increase in Mo enrichment may indicate increased H_2S concentrations and this in turn may be due to a lack of water column Fe that could remove sulfur in the form of pyrite. This Mo increase may have driven the dissolution of P, allowing it to escape the sediment to be recycled higher in the water column. The high C/N ratios (which is also present in chemofacies B) coupled with the dissolution of P suggest that productivity became nitrogen limited, resulting in the preferential removal of nitrogen bearing compounds from the organic matter. This process may also be responsible for the negative $\delta^{15}N$ values that are observed in this chemofacies. Alternatively, the large C/N ratios and negative nitrogen isotope delta values could also have been influenced by slow sedimentation rates that would have allowed more time for the more labile nitrogen bearing compounds in the organic matter to be decomposed.

Chemofacies D

Chemofacies D is identified by a large positive carbon isotope excursion, a sudden decrease in TOC, and decreases in redox-sensitive and bioessential trace metals. Elevated Mn concentrations indicate that this interval was deposited under oxic to suboxic conditions (Figure 4.8). Productivity drops rapidly in this facies (Figure 4.9) but recovers after the carbon isotope excursion along with the abundance of TOC. Modest enrichments in U, and V accompanied by depleted Mo concentrations indicate that sub-oxic conditions existed in the water column.

The deposition of the Eagle Ford coincides with the oceanic anoxic event OAE-2. This worldwide event has been identified by a 3‰ positive shift in the carbon isotope ratio of organic matter in marine sediments (Arthur et al., 1988). The presence of this isotope excursion at the Lake Waco-South Bosque contact (chemofacies C to D) correlates with this event. However, oceanic anoxic events are typically identified by high TOC values rather than the lower values seen in this interval in central Texas. None-the-less, a Cretaceous section at Pueblo, Co. shows a similar trend of declining TOC concurrent with the positive carbon isotope excursion (Pratt and Threlkeld, 1984). There have also been studies which have identified an increase in Mn at or just below this carbon isotope excursion (Pratt et al., 1991) similar to the trend in Mn observed in this study. Based on these similarities, it appears that chemofacies D represents the C/T boundary anoxic event – although suboxic conditions rather than anoxia existed on the shelf where the Eagle Ford was being deposited. Furthermore, it has been noted that the C/T interval for other areas of the Western Interior Seaway display only modest enrichments of TOC in sediments, despite having high primary production rates for the time interval (Meyers et al., 2001, 2005).

It has been reported that "black shales" deposited during the C/T boundary interval typically exhibit $\delta^{15}N$ values, ranging from +1.2‰ to -3.9‰, and atomic carbon/nitrogen (C/N) ratios of 25–50 (Junium and Arthur, 2007) and these are similar to attributes of organic matter in chemofacies B. The negative $\delta^{15}N$ values (Figure 4.10) are probably indicative of fixation of nitrogen from the atmosphere by cyanobacteria. The need for increased fixation of atmospheric nitrogen most likely arose from the removal of dissolved inorganic nitrogen by bacterial denitrification and anaerobic oxidation of ammonia (Sachs and Repeta, 1999; Kuypers et al., 2004). An ecosystem that would favor the fixation of atmospheric nitrogen would be one where nitrogen is the biolimiting nutrient while other nutrients such as phosphorus were readily available (Karl et al., 2002). This may occur in areas of upwelling where oxygen minimum zones occur.

Current theories explaining oceanic anoxic events suggest that they are due to an abrupt rise in temperature due to a rapid influx of CO_2 into the atmosphere from volcanogenic or methanogenic sources (Jenkyns, 2010). The oceanic anoxic event OAE-2 is now thought to be related to increased volcanism (Turgeon and Creaser, 2008). The prevalence of bentonite layers present in chemofacies D supports this idea.

Chemofacies E and F

Chemofacies E represents similar redox and productivity conditions as chemofacies D but lacks the distinctive carbon isotope excursion. These suboxic waters then evolved into the oxic and low-productivity conditions of chemofacies F (Arcadia Park Formation) as indicted by the low concentrations of redox sensitive and bioessential metals suggest a return to normal marine conditions. The source of clastic material during the deposition of this upper most unit remained the same based on the Nb/Ti ratios.

CHAPTER SIX

Conclusions

The use of organic and inorganic geochemical data is an effective method for reconstructing the paleoceanographic conditions which affect the accumulation of organic matter. In addition, these data are also useful for correlation between outcrops. The composite section constructed from outcrops of the Eagle Ford and Pepper Formations indicates the paleoceanographic conditions were quite different between the two formations. Six chemofacies were identified on the basis of the concentrations of major and trace elements, organic matter abundance, $\delta^{13}C_{org}$, $\delta^{15}N_{org}$, and organic matter C/N ratios. These chemofacies were interpreted as the result of changing paleoceanograhic conditions during deposition.

The Pepper Formation is a black, fissile, non-calcareous claystone with a low TOC (avg. 1 wt. %) content and displays little to no enrichment in redox and paleo-productivity trace elements. In contrast, the Eagle Ford Formation is a calcareous silty mudstone with interbedded limestone lenses and laterally continuous bentonite layers. The mudrocks in the Lake Waco member of the Eagle Ford display a high TOC content (avg. 6 wt. %), and enrichments in redox-sensitive and bioessential trace elements, negative nitrogen isotope ratios, and high C/N ratios. Taken together, these data suggest that oceanographic conditions during deposition were euxinic, possibly due to the consumption and subsequent depletion of dissolved oxygen by bacterial degradation of the large amounts of organic matter being produced in the photic zone. The high productivity during this time was likely driven by high nutrient availability, possibly from the upwelling of nutrient rich water from the deep ocean. Nitrogen was most likely the bio-limiting nutrient during this time.

The South Bosque member of the Eagle Ford displays a distinctive positive carbon isotope excursion at its base which corresponds with low to moderate (avg. 4 wt. %) TOC content and only minor enrichments in redox and bioessential trace elements. This positive carbon isotope excursion appears to correlate to the C/T boundary event OAE-2, although the moderate organic matter concentrations and lack of redox-sensitive trace metal indicate that suboxic conditions persisted during this time. This is consistent with the results of other studies of this interval in the Western Interior Seaway. Finally, the deposition of the Arcadia Park Formation marks the return to normal marine conditions.

APPENDICES

APPENDIX A

Outcrop Descriptions and Measured Sections

Outcrop Ch1B

Outcrop Ch1B (31° 04' 49.83" N, 97° 24' 22.81" W) is located on the western slope of a hill on Battle Dr. on the outskirts of the town of Temple, Texas. The outcrop appeared to have some evidence of weathering on the surface, so a small trench was dug in order to obtain fresh material. The first 65cm of this outcrop was a massive, light gray, calcareous siltstone with some scattered shell debris. The rocks in this section react to HCl. The remaining section above 65cm was a dark gray to black, laminated silty claystone. Gypsum crystals and iron staining is present along fracture surfaces. The top of the section was covered.

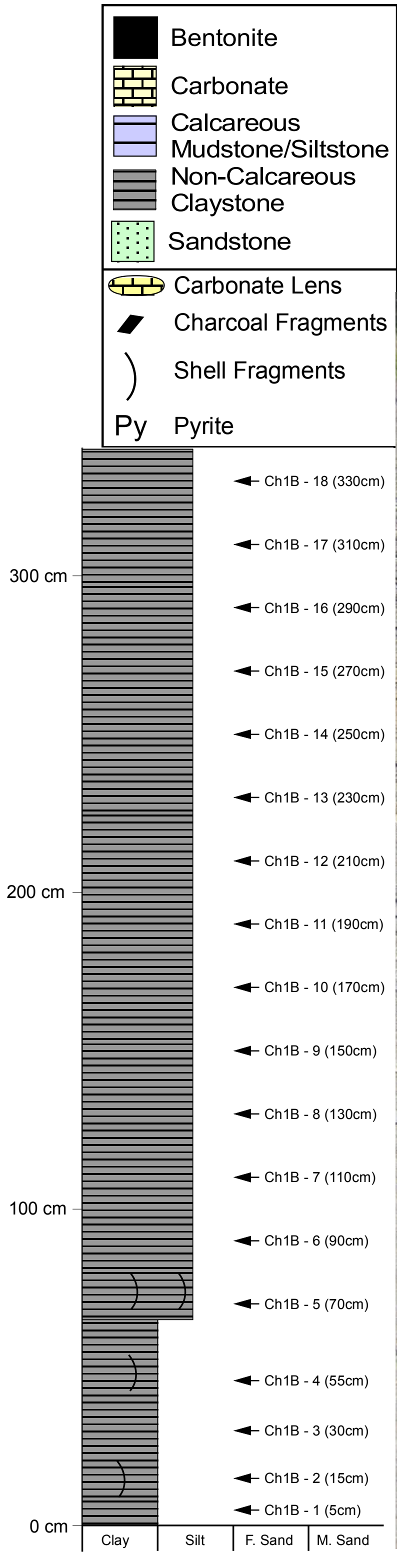

Figure A.1. Outcrop Ch1B stratigraphic column.

Figure A.2. Outcrop Ch1B trench.

Outcrop H/B

Outcrop H/B (31° 28' 33.37" N, 97° 16' 21.80" W) is a former railroad cut which is located on what is now a bike path, just off of Old Lorena Rd. in Woodway. The outcrop appeared to be heavily weathered and had to be trenched in order to obtain unweathered samples. The section from the base of the outcrop to 370cm was a black, laminated claystone. Tiny pyrite crystals are visible in some places. Two thin (~2cm) wavey layers of light gray, fine sand occur within this part of the section. At 370cm from the base of the section a sharp change in lithology occurs. The contact is slightly wavey and was identified as the unconformity surface which separates the Pepper Formation and the Eagle Ford. Above this contact the sediment is much coarser grained, it is a tan to grayish-tan, silty to fine grained, carbonaceous sandy siltstone. This upper part of the section contains shell fragments and several discontinuous carbonate layers and lenticular carbonate flags, many of which appear to have been recrystallized. Scattered fragments of terrestrial plant remains are also seen in this part of the section. Two bentonite layers are visible toward the top of the section.

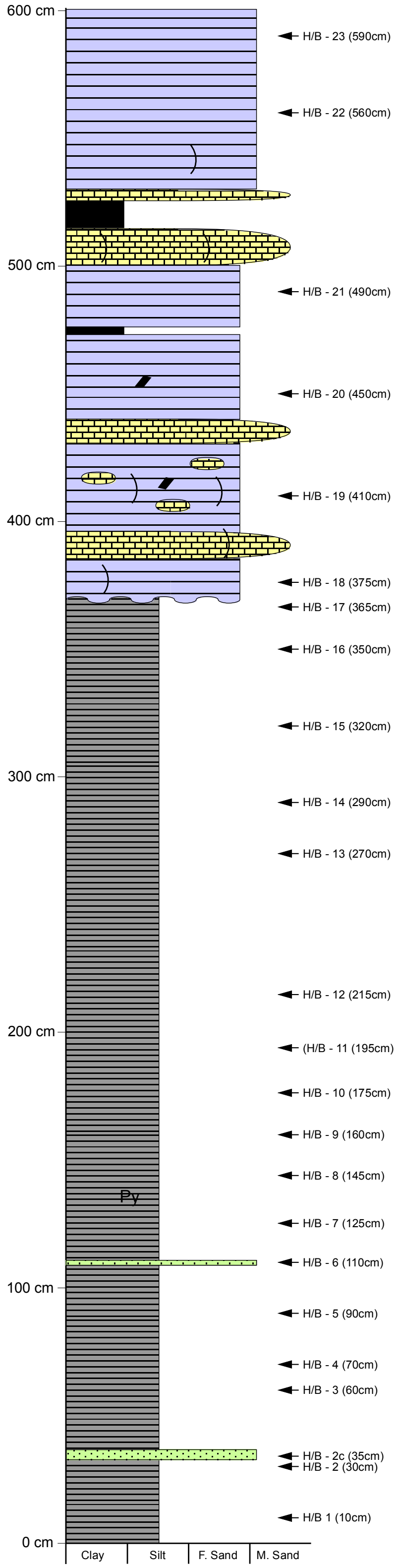

Figure A.3. Outcrop H/B stratigraphic column.

Figure A.4. Outcrop H/B trench.

Outcrop UB

Outcrop UB (31° 21' 27.23" N, 97° 17' 39.58" W) is located under a bridge on Mackey Ranch Rd. in Bruceville-Eddy. This outcrop is fairly cohesive and seems to be resistant to weathering. This section is primarily dominated by a dark-gray, finely laminated, carbonaceous, siltstone. Isolated lenticular carbonate flags occur throughout the section in addition to more continuous carbonate layers. Some of these continuous carbonate layers have scoured bases and appear to fine upwards. The contains abundant fish scales, as well as shell (*Inoceramus*) and bone fragments. Terrestrial plant fragments are also scattered throughout the section. These shell fragments are most concentrated in the carbonate layers and flags. These appear to be storm deposits or turbidities. Several laterally continuous bentonites occur throughout the section. These tend to be more prevalent toward the top of the outcrop.

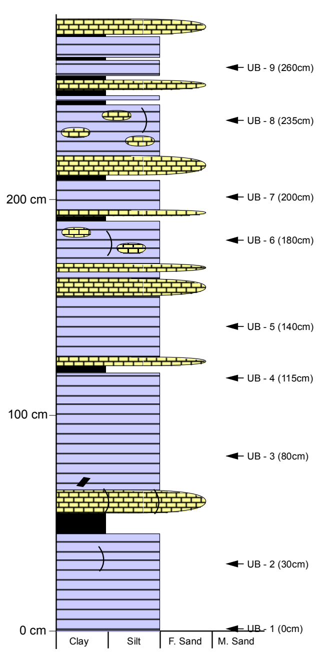

Figure A.5. Outcrop UB stratigraphic column. Figure A.6. Outcrop UB carbonate lenses.

Outcrop UBDS

Outcrop UBDS (31° 21' 8.18" N, 97° 17' 20.62" W) is located about ¾ of a kilometer downstream from outcrop UB. This outcrop was determined to be stratigraphically above the UB outcrop, however the exact vertical distance between the two is unknown. The first 80cm of this outcrop is a thinly laminated, dark gray to black clay rich siltstone. This part of the outcrop contains many small, lenticular, interbedded carbonate flags, most of which have been heavily recrystallized. Several discontinuous bentonites occur within this interval. Above 80cm the carbonate flags are notably absent. The top of this outcrop is capped by a laterally continuous resistive carbonate layer.

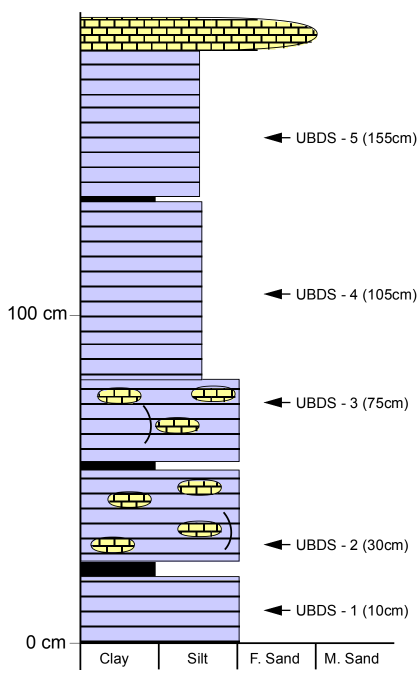

Figure A.7. Outcrop UBDS stratigraphic column. Figure A.8. Outcrop UBDS carbonate lenses.

Outcrop HD

Outcrop HD (31°30'31.30"N, 97°14'28.99"W)is located along a large stream cut behind a housing development off of Stone Lake Drive in Woodway. The base of the section is a dark gray to black, fissile, laminated siltstone. Scattered phosphatic fish scale fragments are common. Several discontinuous limestone and bentonite layers occur in this part of the section. The limestones commonly contain inoceramus shell debris and may form lenticular "flags". A shift in grain size occurs at around 290cm to a dark gray to black, thinly laminated, silty mudstone. This also appears to correspond with a decrease in the number and thickness of limestones. At around 380cm the grain size decreases again to a black laminated mudstone with extremely thin (>1mm) interbedded silty layers. Pyrite crystals can be seen in some places in this interval. At 600cm the mudstone becomes siltier and rare intact inoceramus shells could be found through this interval. Beginning at 660cm the limestones start to reappear as thin discontinuous layers. A partial fish fossil was found at 670cm and a mild hydrocarbon odor was released from these rocks when broken. At 755cm a continuous limestone layer occurs. This layer contains a considerable of pyrite. At about 845cm a 50cm succession of thick (10-15cm) bentonites occurs. These bentonites are separated by limestones which contain scattered fish scales and shell debris. Above this interval several thin bentonite layers occur. The remainder of the section from about 950cm and above consists of a dark gray, laminated silty mudstone.

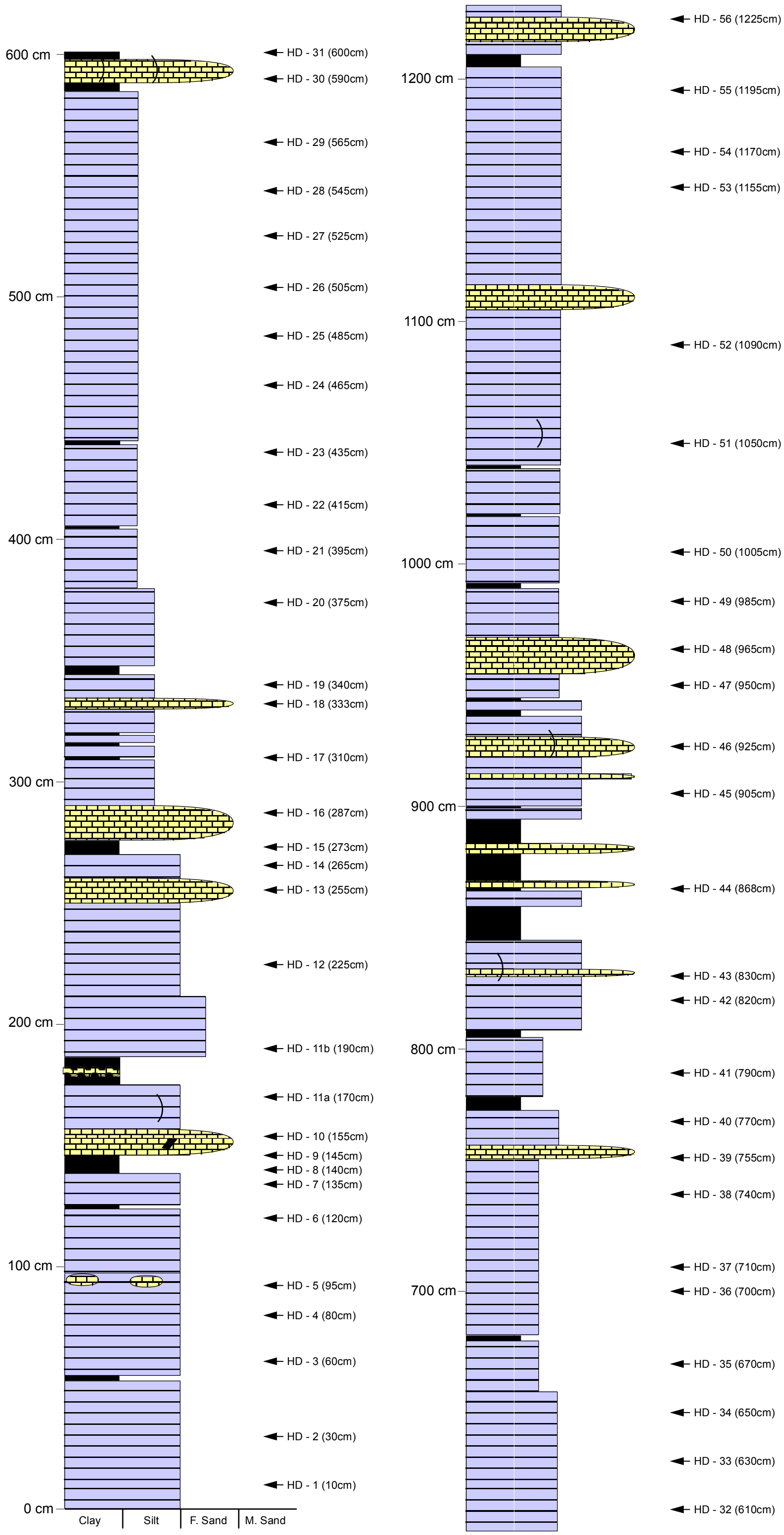

Figure A.9. Outcrop HD stratigraphic column.

Figure A.10. Outcrop HD bentonites.

Outcrop WPDS

Outcrop WPDS (31° 31' 0.60"N, 97° 14' 8.09"W) is located in a stream inside Woodway Park in Woodway. This outcrop appears to be relatively fresh. This outcrop consists primarily of a dark-gray, laminated, silty mudstone. A strong hydrocarbon odor is released from this material when broken. A thin, wavy seam of carbonate rich material occurs 45cm from the base of the outcrop. The remainder of the lower part of this outcrop is devoid of limestone layers, the succession of shale is only broken by a few thin bentonites. At around 200cm the bentonite layers become much more prevalent. Two laterally continuous carbonate layers occur in the upper part of the section. Between 270cm and 310cm a series of thick (up to 10cm) bentonites occur, followed by a series of thinner bentonites towards the top of the section.

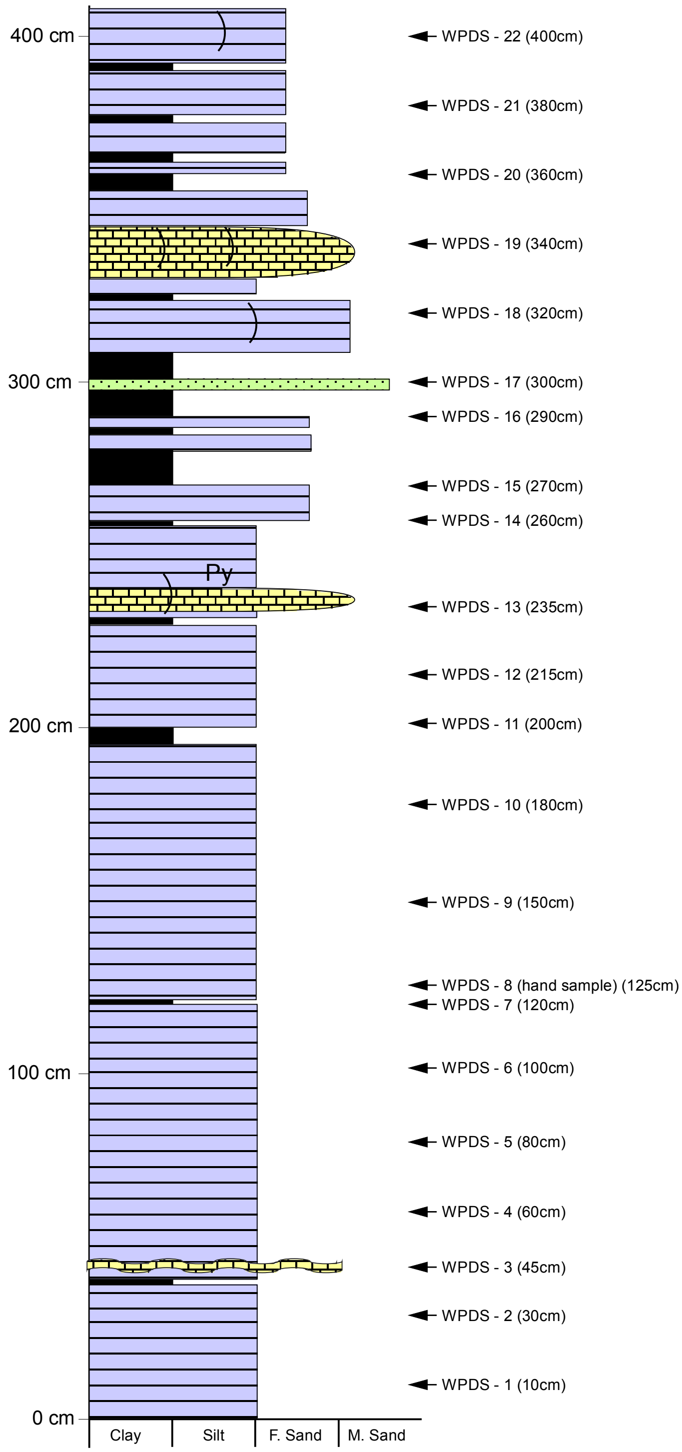

Figure A.11. Outcrop WPDS stratigraphic column.

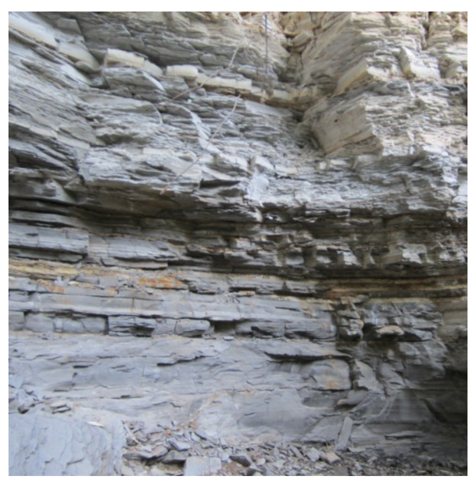

Figure A.12. Outcrop WPDS.

Outcrop WP

Outcrop WP (31° 30' 58.27" N, 97° 14' 3.24" W) is located on a stream cut in Woodway Park in Woodway, TX. This outcrop is upstream from the WPDS outcrop and is separated from it by a normal fault. It was determined to be up-section from the WPDS outcrop. This outcrop displays some unique features which were not recorded at any other outcrops in this study. The base of this outcrop is a dark gray, laminated siltstone. At 55cm the rock changes to a light gray, sandy siltstone which has some evidence of bioturbation. From 65cm to 120cm at least three light gray, laterally continuous bentonite layers occur. These bentonites are separated by massive, muddy limestones which seem to display some bioturbation as pyritized burrows. Directly above these bentonites is a gray, silty, laminated calcareous mudstone with interlaminated siltstones and *inoceramus* fossil fragments. At about 140cm a 5cm thick light gray, wavy, fine sandstone occurs containing terrestrial plant fragments and shell debris. At 150cm is a whitish gray, limestone which has a sharp wavy contact at the base and appears to grade from massive to laminated at the top. Above 160cm is a gray, laminated, fine sandy, fissile siltstone which contains several thin (2-3cm) discontinuous bentonites as well as an abundance of fish vertebrae and *inoceramus* shells. At 230cm a 4cm thick, wavy, intraclastic (bentonitic), sandy, siltstone occurs. This layer contains many well rounded, pebble sized, bentonite intraclasts as well as an abundance of shark and fish teeth. It is bounded above and below by gray laminated siltstones which are separated by sharp, wavy contacts. Just above this layer is a dull, black material that appears to be pure organic matter (picture). This layer was analyzed for organic carbon and nitrogen and was determined to be 65.93% organic carbon and 0.99% organic nitrogen. An elemental analysis was also performed on a sample of this material. It was determined that it is enriched in certain trace metals, most notably vanadium (1901ppm). At 240cm a gray, finely laminated, fissile siltstone occurs which contains several thin (1-2cm) discontinuous bentonites. This layer appears to grade into a massive argillaceous limestone which is capped by a thick (10-13cm) bentonite. Above 300cm is a series of alternating calcareous siltstones and limestones.

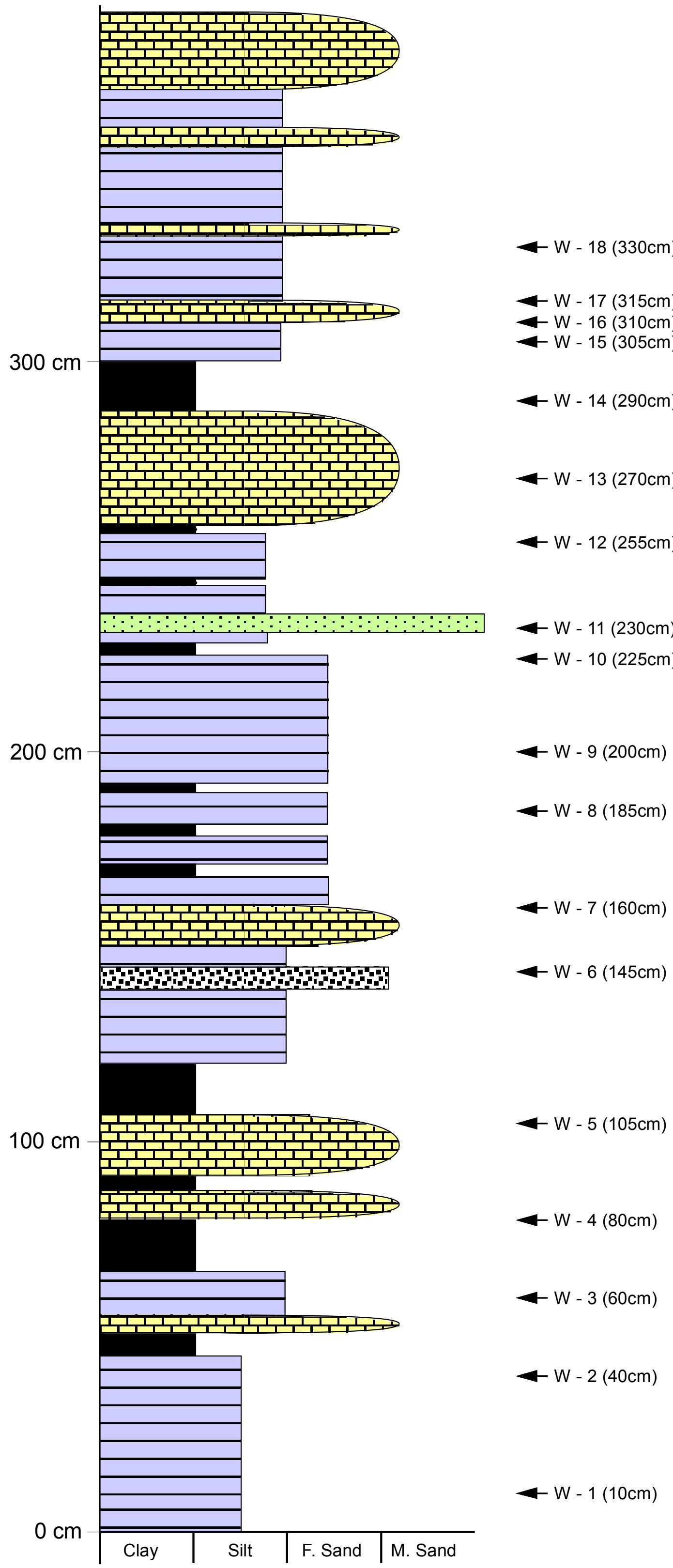

Figure A.13. Outcrop WP stratigraphic column.

Figure A.14. Outcrop WP outcrop picture.

Figure A.15. Outcrop WP asphaltene.

Outcrop C11

Outcrop C11 (31°19'44.33"N, 97°17'40.72"W) is located off of Winchester Dr. in Bruceville-Eddy. This small outcrop consists of a gray, laminated siltstone with scattered shell debris. The outcrop appears to shift to a lighter gray color towards the top, most likely due to increasing carbonate content (this was later confirmed by the geochemical analysis). A few small, black vitreous, lenticular structures were noted in this outcrop. These appear to be pure organic matter and were tentatively described as ashphaltenes. A sample of this material (C11-2a) was analyzed for carbon and nitrogen content and was determined to be 53.18% organic carbon and 1.01% organic nitrogen. A thin (1cm) bentonite was also noted in this section.

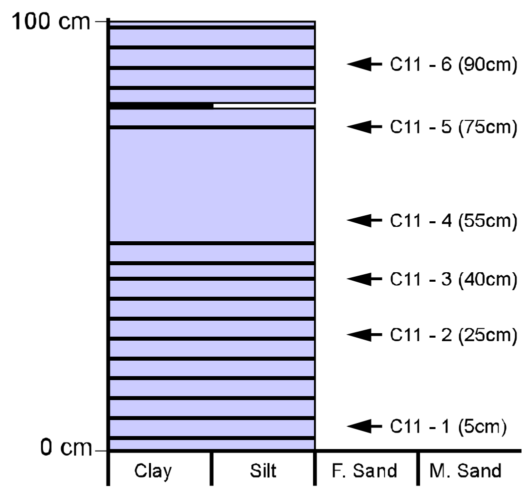

Figure A.16. Outcrop C11 stratigraphic column.

Outcrop EF/AC

Outcrop EF/AC (31°20'1.11"N, 97°13'47.25"W) is located in a small stream cut off of 1st St. in Bruceville-Eddy. This outcrop contains the contact between the Eagle Ford and the overlying Austin Chalk. The lower section of this outcrop is a black, laminated claystone. The contact with the Austin chalk is sharp and slightly undulatory. Vertical and horizontal *trypanites* burrows extend down into the Eagle Ford from the Austin Chalk up to about 20cm from the contact. These burrows have been infilled with material from the Austin. Some horizontal burrows are also present Above the contact the Austin Chalk is highly fossiliferous.

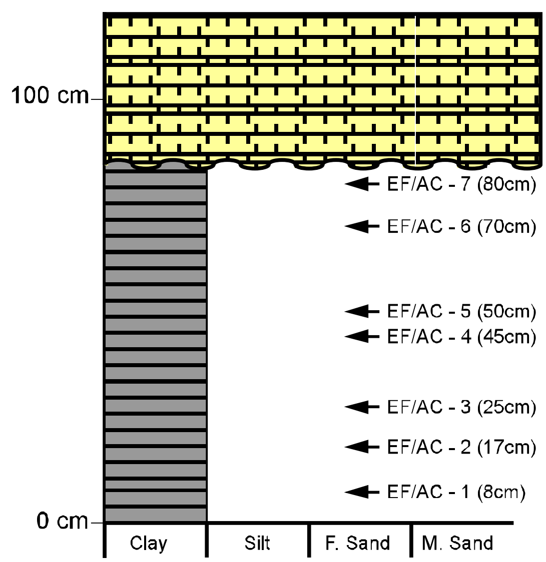

Figure A.17. Outcrop EF/AC stratigraphic column.

Figure A.18. Outcrop EF/AC Austin chalk Eagle Ford (Arcadia Park) contact.

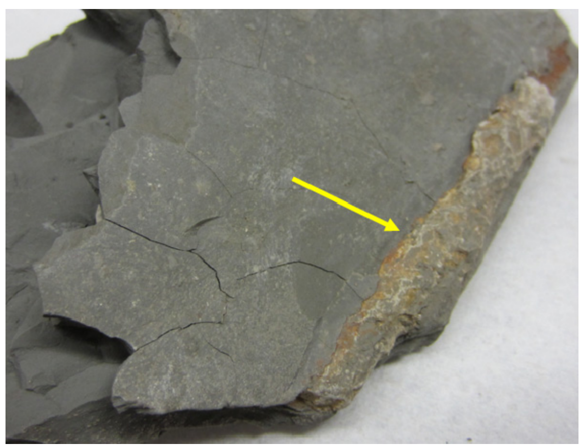

Figure A.19. Outcrop EF/AC trypanites burrows infilled with material from the overlying Austin chalk.

APPENDIX B

Geochemical Data

Table B.1. Organic geochemical data for all samples.

ID #	Sample Name	General Lithology	Outcrop Sample Position (cm)	$\delta^{13}C_{org.}$	$\delta^{15}N$	Total Organic Carbon (wt. %)	Total Nitrogen (wt. %)
1	CH1B-1	Mudrock	5	-25.76	0.71	0.28	0.04
2	CH1B-2	Mudrock	15	-26.16	1.16	0.26	0.03
3	CH1B-3	Mudrock	30	-26.46	-0.76	0.17	0.02
4	CH1B-4	Mudrock	55	-26.36	1.98	0.34	0.04
5	CH1B-5	Mudrock	70	-27.86	0.06	1.99	0.10
6	CH1B-6	Mudrock	90	-27.05	1.48	1.01	0.08
7	CH1B-7	Mudrock	110	-27.55	0.78	1.95	0.11
8	CH1B-8	Mudrock	130	-27.59	0.50	2.00	0.11
9	CH1B-9	Mudrock	150	-27.44	1.13	1.57	0.10
10	CH1B-10	Mudrock	170	-27.17	1.19	1.06	0.08
11	CH1B-11	Mudrock	190	-26.93	1.33	0.90	0.07
12	CH1B-12	Mudrock	210	-27.08	1.34	0.98	0.07
13	CH1B-13	Mudrock	230	-27.20	1.18	1.04	0.08
14	CH1B-14	Mudrock	250	-27.08	1.48	0.94	0.07
15	CH1B-15	Mudrock	270	-27.26	1.68	1.02	0.07
16	CH1B-16	Mudrock	290	-27.24	1.53	0.94	0.07
17	CH1B-17	Mudrock	310	-27.07	1.17	1.00	0.07
18	CH1B-18	Mudrock	330	-27.09	1.30	0.98	0.07
19	H/B-1	Mudrock	10	-27.32	1.32	1.77	0.10
20	H/B-2	Mudrock	30	-26.82	1.37	1.33	0.08
21	H/B-2c	Sandstone	35	-26.63	-0.32	0.54	0.04
22	H/B-3	Mudrock	60	-27.37	1.17	1.67	0.08
23	H/B-4	Mudrock	70	-26.92	1.76	1.62	0.09
24	H/B-5	Mudrock	90	-27.31	1.45	1.50	0.09
25	H/B-6	Mudrock	110	-27.39	2.18	1.77	0.09
26	H/B-7	Mudrock	125	-27.59	1.78	1.57	0.10
27	H/B-8	Mudrock	145	-27.54	1.70	1.51	0.09
28	H/B-9	Mudrock	160	-27.35	1.87	1.51	0.09
29	H/B-10	Mudrock	175	-27.40	1.74	1.51	0.09
30	H/B-11	Mudrock	195	-27.30	2.44	1.50	0.09
31	H/B-12	Mudrock	215	-27.56	1.41	1.24	0.08
32	H/B-13	Mudrock	270	-27.68	1.29	1.29	0.09

Table B.1 continued

ID #	Sample Name	General Lithology	Outcrop Sample Position (cm)	$\delta^{13}C_{org.}$	$\delta^{15}N$	Total Organic Carbon (wt. %)	Total Nitrogen (wt. %)
33	H/B-14	Mudrock	290	-27.87	0.51	1.44	0.08
34	H/B-15	Mudrock	320	-27.73	-0.78	1.11	0.08
35	H/B-16	Mudrock	350	-27.92	-0.24	1.13	0.08
36	H/B-17	Mudrock	365	-27.85	-0.68	0.97	0.08
37	H/B-18	Mudrock	375	-26.10	-1.98	4.42	0.18
38	H/B-19	Mudrock	410	-26.51	-1.62	1.61	0.07
39	H/B-20	Mudrock	450	-27.43	-0.92	4.48	0.18
40	H/B-21	Mudrock	490	-26.90	-0.76	5.43	0.20
41	H/B-22	Mudrock	560	-27.15	-0.66	4.29	0.18
42	H/B-23	Mudrock	590	-27.46	-0.84	3.31	0.14
43	UB-1	Mudrock	0	-27.31	-1.77	6.13	0.24
44	UB-2	Mudrock	30	-27.55	-1.68	7.70	0.30
45	UB-3	Mudrock	80	-27.67	-2.13	4.72	0.20
46	UB-Org.	Organics	85	-25.64	1.20	56.67	1.61
47	UB-4	Mudrock	115	-27.27	-1.61	7.90	0.32
48	UB-5	Mudrock	140	-27.71	-2.01	5.70	0.23
49	UB-6	Mudrock	180	-27.68	-3.38	4.07	0.17
50	UB-7	Mudrock	200	-27.47	-2.52	5.16	0.19
51	UB-8	Mudrock	235	-27.66	-3.31	3.36	0.13
52	UB-9	Mudrock	290	-27.97	-2.28	5.75	0.21
53	UBDS-1	Mudrock	10	-27.18	-1.68	9.49	0.35
54	UBDS-2	Mudrock	30	-27.41	-1.97	8.72	0.32
55	UBDS-3	Mudrock	75	-27.84	-3.53	4.22	0.18
56	UBDS-4	Mudrock	105	-27.72	-2.45	7.27	0.29
57	UBDS-5	Mudrock	155	-27.60	-2.69	4.81	0.20
58	HD-1	Mudrock	10	-27.73	-1.42	4.95	0.20
59	HD-2	Mudrock	30	-27.63	-1.32	6.18	0.24
60	HD-3	Mudrock	60	-27.99	-1.47	5.82	0.23
61	HD-4	Mudrock	80	-27.87	-1.70	5.11	0.20
62	HD-5	Limestone	95	-27.58	-3.51	0.97	0.03
63	HD-6	Mudrock	120	-27.70	-1.09	3.84	0.14
64	HD-7	Mudrock	135	-27.66	-1.16	4.48	0.17
65	HD-8	Limestone	140	-25.49	-2.86	0.05	0.01
66	HD-9	Bentonite	145	-26.79	-2.35	0.42	0.02
67	HD-10	Limestone	155	-27.54	-4.55	0.75	0.03
68	HD-11A	Mudrock	170	-27.38	-1.48	2.12	0.09
69	HD-11B	Mudrock	190	-27.87	-1.85	5.18	0.18
70	HD-12	Mudrock	225	-27.77	-3.16	4.82	0.16

Table B.1 continued

ID #	Sample Name	General Lithology	Outcrop Sample Position (cm)	$\delta^{13}C_{org.}$	$\delta^{15}N$	Total Organic Carbon (wt. %)	Total Nitrogen (wt. %)
71	HD-13	Limestone	255	-27.43	-4.99	1.17	0.03
72	HD-14	Mudrock	265	-27.57	-2.37	4.13	0.14
73	HD-15	Bentonite	273	-26.78	-11.25	0.11	0.01
74	HD-16	Limestone	287	-27.16	-11.33	0.07	0.01
75	HD-17	Mudrock	310	-27.52	-3.19	6.33	0.20
76	HD-18	Limestone	333	-27.97	-4.98	0.43	0.02
77	HD-19	Mudrock	340	-27.65	-3.47	6.51	0.19
78	HD-20	Mudrock	375	-27.48	-2.28	7.35	0.22
79	HD-21	Mudrock	395	-27.42	-2.79	6.37	0.19
80	HD-22	Mudrock	415	-27.30	-2.70	7.39	0.21
81	HD-23	Mudrock	435	-27.11	-2.21	7.69	0.23
82	HD-24	Mudrock	465	-27.61	-2.90	6.32	0.18
83	HD-25	Mudrock	485	-27.43	-1.97	7.24	0.21
84	HD-26	Mudrock	505	-27.40	-2.68	6.60	0.20
85	HD-27	Mudrock	525	-27.40	-2.65	7.34	0.22
86	HD-28	Mudrock	545	-27.69	-2.73	6.31	0.20
87	HD-29	Mudrock	565	-27.42	-2.66	7.10	0.22
88	HD-30	Limestone	590	-25.13	-3.15	1.43	0.05
89	HD-31	Limestone	600	-27.43	-7.34	0.16	0.01
90	HD-32	Mudrock	610	-27.55	-2.98	4.71	0.14
91	HD-33	Mudrock	630	-27.36	-3.25	5.53	0.16
92	HD-34	Mudrock	650	-27.34	-3.16	5.53	0.15
93	HD-35	Mudrock	670	-27.35	-2.84	6.21	0.18
94	HD-36	Mudrock	700	-27.06	-3.20	6.20	0.16
95	HD-37	Mudrock	710	-26.95	-3.00	7.60	0.20
96	HD-38	Mudrock	740	-27.22	-3.17	7.13	0.18
97	HD-39	Limestone	755	-28.17	-6.98	0.61	0.03
98	HD-40	Mudrock	770	-26.93	-1.17	6.97	0.24
99	HD-41	Mudrock	790	-26.73	-2.62	8.00	0.25
100	HD-42	Mudrock	820	-26.91	-2.52	6.06	0.18
101	HD-43	Limestone	830	-26.56	-3.89	0.98	0.05
102	HD-44	Limestone	868	-26.65	-4.07	0.38	0.01
103	HD-45	Mudrock	905	-27.47	-2.11	5.06	0.16
104	HD-46	Limestone	925	-26.88	-4.55	0.77	0.02
105	HD-47	Mudrock	950	-27.62	-3.05	8.19	0.25
106	HD-48	Limestone	965	-27.20	-6.40	0.61	0.04
107	HD-49	Mudrock	985	-27.82	-3.69	5.50	0.16
108	HD-50	Mudrock	1005	-27.62	-3.02	6.82	0.22

Table B.1 continued

ID #	Sample Name	General Lithology	Outcrop Sample Position (cm)	$\delta^{13}C_{org.}$	$\delta^{15}N$	Total Organic Carbon (wt. %)	Total Nitrogen (wt. %)
109	HD-51	Mudrock	1050	-27.70	-3.14	5.24	0.18
110	HD-52	Mudrock	1090	-27.43	-2.61	5.91	0.18
111	HD-53	Mudrock	1155	-27.69	-4.09	3.49	0.11
112	HD-54	Mudrock	1170	-27.70	-2.94	5.99	0.18
113	HD-55	Mudrock	1195	-28.09	-2.45	5.12	0.18
114	HD-56	Limestone	1225	-27.61	-2.70	0.77	0.05
115	WPDS-1	Mudrock	10	-27.74	-2.89	6.62	0.24
116	WPDS-2	Mudrock	30	-27.60	-2.78	6.68	0.22
117	WPDS-3	Limestone	45	-27.62	-3.89	1.43	0.06
118	WPDS-4	Mudrock	60	-27.85	-1.84	5.70	0.19
119	WPDS-5	Mudrock	80	-27.63	-3.15	6.69	0.21
120	WPDS-6	Mudrock	100	-27.38	-3.19	6.22	0.19
121	WPDS-7	Mudrock	120	-27.68	-3.02	5.78	0.18
122	WPDS-8	Mudrock	125	-27.75	-3.71	3.39	0.10
123	WPDS-9	Mudrock	150	-27.11	-1.18	6.45	0.22
124	WPDS-10	Mudrock	180	-27.33	-2.97	6.41	0.20
125	WPDS-11	Mudrock	200	-26.77	-3.30	6.51	0.21
126	WPDS-12	Mudrock	215	-26.94	-2.94	7.18	0.23
127	WPDS-13	Limestone	235	-26.68	-5.08	0.89	0.04
128	WPDS-14	Mudrock	260	-26.84	-2.36	6.14	0.19
129	WPDS-15	Mudrock	270	-26.89	-3.14	7.21	0.22
130	WPDS-16	Mudrock	290	-26.83	-5.01	1.64	0.06
131	WPDS-17	Mudrock	300	-26.94	-6.13	1.14	0.04
132	WPDS-18	Mudrock	320	-27.34	-3.23	4.72	0.15
133	WPDS-19	Limestone	340	-26.94	-2.09	0.75	0.03
134	WPDS-20	Mudrock	360	-27.57	-3.97	3.35	0.12
135	WPDS-21	Mudrock	380	-27.83	-3.89	3.33	0.11
136	WPDS-22	Mudrock	400	-27.54	-3.22	6.44	0.19
137	WP-1	Mudrock	10	-27.40	-1.81	3.44	0.15
138	WP-2	Mudrock	40	-26.98	-2.35	2.46	0.12
139	WP-3	Mudrock	60	-24.28	-5.98	0.88	0.07
140	WP-4	Limestone	80	-24.10	-1.40	0.14	0.03
141	WP-5	Limestone	105	-24.24	-9.15	0.09	0.01
142	WP-6	Mudrock	145	-24.17	-3.42	0.40	0.03
143	WP-7	Limestone	160	-24.34	-8.63	0.23	0.01
144	WP-8	Mudrock	185	-24.01	-3.63	2.93	0.13
145	WP-9	Mudrock	200	-24.08	-4.40	1.19	0.05
146	WP-10	Mudrock	225	-24.02	-2.83	2.05	0.10

Table B.1 continued

ID #	Sample Name	General Lithology	Outcrop Sample Position (cm)	$\delta^{13}C_{org.}$	$\delta^{15}N$	Total Organic Carbon (wt. %)	Total Nitrogen (wt. %)
147	WP-11	Conglomerate	230	-24.16	-3.38	0.19	0.02
148	WP-Org.	Organics	230	-22.99	0.37	65.93	0.99
149	WP-12	Mudrock	255	-24.85	-2.78	4.29	0.18
150	WP-13	Limestone	270	-24.06	-4.81	1.38	0.05
151	WP-14	Bentonite	290	-26.28	-17.32	0.04	0.01
152	WP-15	Mudrock	305	-25.68	-3.93	2.10	0.10
153	WP-16	Mudrock	310	-26.34	-2.98	1.72	0.09
154	WP-17	Limestone	315	-25.76	-4.61	0.31	0.03
155	WP-18	Mudrock	330	-26.90	-2.09	4.93	0.21
156	C11-1	Mudrock	0	-27.32	-0.76	3.76	0.16
157	C11-2	Mudrock	25	-27.58	-1.02	2.93	0.12
158	C11-2 Org.	Organics	25	-26.04	1.05	53.18	1.02
159	C11-3	Mudrock	40	-27.52	-0.47	3.63	0.16
160	C11-4	Mudrock	55	-27.53	-0.62	2.15	0.09
161	C11-5	Mudrock	75	-27.28	-0.93	1.26	0.06
162	C11-6	Mudrock	90	-27.60	-1.21	0.99	0.05
163	EFAC-1	Mudrock	5	-27.18	-2.24	0.78	0.08
164	EFAC-2	Mudrock	15	-27.09	-1.19	0.82	0.08
165	EFAC-3	Mudrock	25	-27.20	-2.85	0.82	0.09
166	EFAC-4	Mudrock	40	-27.26	-1.81	0.91	0.09
167	EFAC-5	Mudrock	50	-27.24	1.50	0.87	0.08
168	EFAC-6	Mudrock	70	-27.21	1.15	0.90	0.08
169	EFAC-7	Mudrock	80	-27.24	-1.01	0.94	0.08

Table B.2. Major element concentrations for all samples part 1

ID #	Sample Name	General Lithology	Outcrop Sample Position (cm)	SiO_2 (wt. %)	TiO_2 (wt. %)	Al_2O_3 (wt. %)	Fe_2O_3 (wt. %)	MnO (wt. %)
1	CH1B-1	Mudrock	5	59.573	0.731	15.210	4.721	0.032
2	CH1B-2	Mudrock	15	57.831	0.599	13.993	4.386	0.050
3	CH1B-3	Mudrock	30	46.144	0.318	8.752	3.270	0.120
4	CH1B-4	Mudrock	55	58.268	0.633	14.240	4.695	0.047
5	CH1B-5	Mudrock	70	55.740	0.789	17.570	5.602	0.051
6	CH1B-6	Mudrock	90	56.034	0.988	19.051	5.123	0.047
7	CH1B-7	Mudrock	110	61.364	0.959	18.985	3.944	0.015
8	CH1B-8	Mudrock	130	61.053	0.960	19.343	4.078	0.014
9	CH1B-9	Mudrock	150	60.743	1.032	18.954	3.910	0.012

Table B.2 Continued

ID #	Sample Name	General Lithology	Outcrop Sample Position (cm)	SiO_2 (wt. %)	TiO_2 (wt. %)	Al_2O_3 (wt. %)	Fe_2O_3 (wt. %)	MnO (wt. %)
10	CH1B-10	Mudrock	170	58.904	1.043	19.543	4.239	0.015
11	CH1B-11	Mudrock	190	62.168	1.138	19.296	3.687	0.013
12	CH1B-12	Mudrock	210	59.496	1.080	18.224	3.790	0.009
13	CH1B-13	Mudrock	230	62.167	1.009	19.393	3.717	0.009
14	CH1B-14	Mudrock	250	62.036	1.044	20.146	3.543	0.010
15	CH1B-15	Mudrock	270	59.565	0.990	19.237	4.245	0.017
16	CH1B-16	Mudrock	290	62.944	1.029	19.809	3.767	0.009
17	CH1B-17	Mudrock	310	62.321	1.053	19.587	3.740	0.008
18	CH1B-18	Mudrock	330	64.073	1.047	18.992	3.129	0.009
19	H/B-1	Mudrock	10	65.666	1.188	17.901	4.113	0.009
20	H/B-2	Mudrock	30	68.580	1.195	16.635	3.299	0.008
21	H/B-2c	Sandstone	35	81.878	0.921	11.191	1.776	0.006
22	H/B-3	Mudrock	60	66.637	1.142	17.282	3.379	0.008
23	H/B-4	Mudrock	70	65.032	1.084	17.101	3.669	0.008
24	H/B-5	Mudrock	90	61.170	1.074	16.082	4.813	0.009
25	H/B-6	Mudrock	110	67.397	1.087	16.191	3.406	0.008
26	H/B-7	Mudrock	125	61.927	1.071	17.252	5.205	0.009
27	H/B-8	Mudrock	145	61.788	1.048	17.395	4.732	0.010
28	H/B-9	Mudrock	160	63.062	1.067	17.020	4.160	0.008
29	H/B-10	Mudrock	175	62.878	1.086	17.501	4.158	0.008
30	H/B-11	Mudrock	195	59.454	1.064	16.344	3.780	0.008
31	H/B-12	Mudrock	215	59.425	1.027	15.564	3.480	0.007
32	H/B-13	Mudrock	270	59.343	1.008	15.251	4.651	0.007
33	H/B-14	Mudrock	290	68.006	1.061	15.677	2.878	0.007
34	H/B-15	Mudrock	320	67.628	1.048	15.722	2.785	0.007
35	H/B-16	Mudrock	350	63.895	1.001	15.337	4.064	0.007
36	H/B-17	Mudrock	365	59.280	0.996	15.051	3.309	0.008
37	H/B-18	Mudrock	375	40.591	0.360	10.679	6.155	0.042
38	H/B-19	Mudrock	410	22.573	0.094	6.650	2.852	0.064
39	H/B-20	Mudrock	450	41.597	0.375	10.064	6.385	0.050
40	H/B-21	Mudrock	490	38.737	0.327	9.130	6.025	0.044
41	H/B-22	Mudrock	560	46.927	0.490	11.223	6.707	0.032
42	H/B-23	Mudrock	590	41.149	0.342	9.637	5.881	0.038
43	UB-1	Mudrock	0	39.356	0.325	9.102	5.250	0.033
44	UB-2	Mudrock	30	43.616	0.452	10.791	6.873	0.029
45	UB-3	Mudrock	80	37.227	0.243	8.905	4.284	0.034
46	UB-Org.	Organics	85	-	-	-	-	-
47	UB-4	Mudrock	115	45.969	0.596	11.162	6.930	0.025
48	UB-5	Mudrock	140	42.482	0.340	9.351	5.220	0.031
49	UB-6	Mudrock	180	33.065	0.251	7.317	5.585	0.039
50	UB-7	Mudrock	200	40.372	0.317	8.449	4.692	0.029
51	UB-8	Mudrock	235	25.533	0.171	6.020	3.028	0.043
52	UB-9	Mudrock	290	33.989	0.214	7.612	4.212	0.031
53	UBDS-1	Mudrock	10	37.049	0.306	9.002	4.645	0.029
54	UBDS-2	Mudrock	30	39.569	0.410	10.446	5.746	0.024

Table B.2 Continued

ID #	Sample Name	General Lithology	Outcrop Sample Position (cm)	SiO_2 (wt. %)	TiO_2 (wt. %)	Al_2O_3 (wt. %)	Fe_2O_3 (wt. %)	MnO (wt. %)
55	UBDS-3	Mudrock	75	38.914	0.319	10.448	4.538	0.036
56	UBDS-4	Mudrock	105	38.195	0.308	8.896	5.193	0.028
57	UBDS-5	Mudrock	155	36.269	0.287	8.448	4.969	0.034
58	HD-1	Mudrock	10	41.476	0.331	9.613	5.015	0.038
59	HD-2	Mudrock	30	41.273	0.375	10.144	5.746	0.034
60	HD-3	Mudrock	60	37.105	0.327	9.568	5.730	0.034
61	HD-4	Mudrock	80	30.497	0.223	7.027	4.399	0.038
62	HD-5	Limestone	95	9.953	0.025	2.589	1.723	0.037
63	HD-6	Mudrock	120	32.019	0.260	7.742	4.483	0.036
64	HD-7	Mudrock	135	31.550	0.234	7.334	4.598	0.032
65	HD-8	Limestone	140	22.105	0.053	6.517	1.921	0.065
66	HD-9	Bentonite	145	46.850	0.485	16.560	4.805	0.032
67	HD-10	Limestone	155	10.291	0.028	3.244	1.272	0.040
68	HD-11A	Mudrock	170	39.687	0.266	9.364	4.476	0.036
69	HD-11B	Mudrock	190	32.746	0.186	7.265	3.631	0.034
70	HD-12	Mudrock	225	36.479	0.211	7.220	3.229	0.036
71	HD-13	Limestone	255	12.973	0.030	2.644	1.361	0.026
72	HD-14	Mudrock	265	35.705	0.244	8.079	3.446	0.036
73	HD-15	Bentonite	273	52.452	0.167	16.593	0.936	0.006
74	HD-16	Limestone	287	17.132	-0.013	4.435	2.420	0.044
75	HD-17	Mudrock	310	39.767	0.252	9.217	3.550	0.032
76	HD-18	Limestone	333	8.706	-0.008	2.369	1.157	0.039
77	HD-19	Mudrock	340	38.927	0.245	8.515	3.707	0.031
78	HD-20	Mudrock	375	32.835	0.186	6.323	3.227	0.029
79	HD-21	Mudrock	395	38.658	0.230	7.437	3.695	0.027
80	HD-22	Mudrock	415	37.384	0.251	7.893	3.673	0.028
81	HD-23	Mudrock	435	36.224	0.267	7.883	4.286	0.028
82	HD-24	Mudrock	465	35.955	0.210	7.007	3.270	0.027
83	HD-25	Mudrock	485	39.704	0.257	7.921	3.774	0.029
84	HD-26	Mudrock	505	40.563	0.254	7.759	3.604	0.029
85	HD-27	Mudrock	525	41.118	0.280	8.369	3.606	0.027
86	HD-28	Mudrock	545	42.969	0.279	8.384	3.644	0.026
87	HD-29	Mudrock	565	44.085	0.321	9.025	4.057	0.027
88	HD-30	Limestone	590	17.436	0.029	3.179	1.104	0.035
89	HD-31	Limestone	600	14.440	0.084	4.026	14.495	0.040
90	HD-32	Mudrock	610	37.903	0.225	7.214	3.587	0.027
91	HD-33	Mudrock	630	40.455	0.235	7.344	3.777	0.027
92	HD-34	Mudrock	650	35.895	0.160	5.948	2.777	0.029
93	HD-35	Mudrock	670	38.142	0.212	6.783	3.258	0.027
94	HD-36	Mudrock	700	28.637	0.151	5.246	3.179	0.028
95	HD-37	Mudrock	710	38.652	0.231	7.040	3.536	0.027
96	HD-38	Mudrock	740	32.275	0.187	5.884	3.190	0.030
97	HD-39	Limestone	755	10.901	0.012	2.755	9.017	0.042
98	HD-40	Mudrock	770	35.177	0.209	6.761	3.215	0.030
99	HD-41	Mudrock	790	47.318	0.269	9.240	3.542	0.024

Table B.2 Continued

ID #	Sample Name	General Lithology	Outcrop Sample Position (cm)	SiO_2 (wt. %)	TiO_2 (wt. %)	Al_2O_3 (wt. %)	Fe_2O_3 (wt. %)	MnO (wt. %)
100	HD-42	Mudrock	820	32.646	0.160	5.508	2.866	0.026
101	HD-43	Limestone	830	20.433	0.022	3.755	1.436	0.039
102	HD-44	Limestone	868	27.088	0.232	9.878	3.549	0.058
103	HD-45	Mudrock	905	35.283	0.178	6.545	3.452	0.027
104	HD-46	Limestone	925	15.250	-0.003	1.688	0.629	0.042
105	HD-47	Mudrock	950	36.700	0.190	6.030	3.480	0.027
106	HD-48	Limestone	965	13.787	0.010	3.122	5.020	0.037
107	HD-49	Mudrock	985	35.070	0.210	7.219	3.605	0.027
108	HD-50	Mudrock	1005	29.743	0.155	5.561	3.362	0.031
109	HD-51	Mudrock	1050	24.629	0.119	4.582	2.442	0.026
110	HD-52	Mudrock	1090	24.247	0.099	4.073	2.680	0.025
111	HD-53	Mudrock	1155	21.579	0.092	4.853	2.556	0.028
112	HD-54	Mudrock	1170	26.676	0.125	4.741	3.154	0.025
113	HD-55	Mudrock	1195	27.982	0.105	4.604	2.250	0.024
114	HD-56	Limestone	1225	11.094	-0.005	2.285	1.576	0.046
115	WPDS-1	Mudrock	10	41.430	0.276	8.516	3.934	0.028
116	WPDS-2	Mudrock	30	40.866	0.243	7.903	3.663	0.030
117	WPDS-3	Limestone	45	13.673	0.026	3.115	8.241	0.036
118	WPDS-4	Mudrock	60	33.826	0.176	6.515	3.174	0.029
119	WPDS-5	Mudrock	80	39.204	0.240	7.470	3.303	0.026
120	WPDS-6	Mudrock	100	36.959	0.182	6.383	3.221	0.028
121	WPDS-7	Mudrock	120	37.316	0.194	7.226	3.520	0.029
122	WPDS-8	Mudrock	125	29.009	0.122	5.270	3.185	0.029
123	WPDS-9	Mudrock	150	40.836	0.214	6.763	3.187	0.026
124	WPDS-10	Mudrock	180	35.444	0.193	6.400	3.763	0.030
125	WPDS-11	Mudrock	200	48.453	0.309	11.831	3.693	0.026
126	WPDS-12	Mudrock	215	42.431	0.233	7.536	3.413	0.026
127	WPDS-13	Limestone	235	13.669	0.011	2.613	2.240	0.040
128	WPDS-14	Mudrock	260	39.518	0.191	6.620	3.015	0.026
129	WPDS-15	Mudrock	270	41.978	0.206	7.648	3.301	0.033
130	WPDS-16	Mudrock	290	33.551	0.212	10.344	3.294	0.052
131	WPDS-17	Mudrock	300	46.902	0.101	12.798	3.134	0.036
132	WPDS-18	Mudrock	320	32.115	0.163	6.303	3.446	0.026
133	WPDS-19	Limestone	340	14.689	0.001	1.891	0.916	0.039
134	WPDS-20	Mudrock	360	38.954	0.238	10.379	3.937	0.028
135	WPDS-21	Mudrock	380	35.631	0.216	8.252	3.705	0.028
136	WPDS-22	Mudrock	400	29.247	0.140	5.477	3.321	0.031
137	WP-1	Mudrock	10	51.372	0.387	10.374	4.949	0.023
138	WP-2	Mudrock	40	45.277	0.412	10.981	7.099	0.058
139	WP-3	Mudrock	60	52.683	1.091	16.321	5.893	0.021
140	WP-4	Limestone	80	24.526	0.212	6.143	5.374	0.158
141	WP-5	Limestone	105	15.678	0.123	4.141	2.719	0.157
142	WP-6	Mudrock	145	22.869	0.137	6.650	3.244	0.046
143	WP-7	Limestone	160	12.384	0.011	3.293	0.461	0.101
144	WP-8	Mudrock	185	48.031	0.446	10.442	5.103	0.028

Table B.2 Continued

ID #	Sample Name	General Lithology	Outcrop Sample Position (cm)	SiO_2 (wt. %)	TiO_2 (wt. %)	Al_2O_3 (wt. %)	Fe_2O_3 (wt. %)	MnO (wt. %)
145	WP-9	Mudrock	200	20.941	0.075	4.808	1.900	0.039
146	WP-10	Mudrock	225	48.302	0.496	10.673	4.313	0.028
147	WP-11	Conglomerate	230	14.520	0.115	4.655	7.567	0.036
148	WP-Org.	Organics	230	0.388	1.226	0.463	4.180	0.009
149	WP-12	Mudrock	255	43.706	0.437	9.489	4.241	0.029
150	WP-13	Limestone	270	17.902	0.065	3.435	1.683	0.039
151	WP-14	Bentonite	290	54.206	0.182	16.659	1.351	0.005
152	WP-15	Mudrock	305	43.857	0.267	12.228	2.783	0.025
153	WP-16	Mudrock	310	38.096	0.189	9.954	2.599	0.027
154	WP-17	Limestone	315	26.208	0.095	5.877	2.181	0.035
155	WP-18	Mudrock	330	45.547	0.279	10.610	2.854	0.021
156	C11-1	Mudrock	0	44.459	0.398	11.401	4.371	0.031
157	C11-2	Mudrock	25	42.076	0.321	10.649	4.302	0.027
158	C11-2 Org.	Organics	25	-	-	-	-	-
159	C11-3	Mudrock	40	45.042	0.389	10.727	3.964	0.025
160	C11-4	Mudrock	55	31.748	0.189	7.204	3.620	0.030
161	C11-5	Mudrock	75	30.099	0.156	7.349	3.077	0.031
162	C11-6	Mudrock	90	23.708	0.101	5.428	3.169	0.037
163	EFAC-1	Mudrock	5	59.063	0.901	15.924	5.564	0.026
164	EFAC-2	Mudrock	15	60.525	0.913	15.876	5.401	0.024
165	EFAC-3	Mudrock	25	60.674	0.915	15.934	5.399	0.024
166	EFAC-4	Mudrock	40	59.884	0.905	15.958	5.259	0.024
167	EFAC-5	Mudrock	50	59.700	0.891	15.902	5.363	0.024
168	EFAC-6	Mudrock	70	57.251	0.909	15.409	5.076	0.023
169	EFAC-7	Mudrock	80	60.840	0.871	16.181	5.313	0.024

Table B.3. Major element concentrations for all samples part 2

ID #	Sample Name	General Lithology	Outcrop Sample Position (cm)	MgO (wt. %)	CaO (wt. %)	Na_2O (wt. %)	K_2O (wt. %)	P_2O_5 (wt. %)
1	CH1B-1	Mudrock	5	1.492	8.430	0.158	1.979	0.073
2	CH1B-2	Mudrock	15	1.501	13.847	0.154	1.740	0.104
3	CH1B-3	Mudrock	30	1.410	30.667	0.134	0.904	0.210
4	CH1B-4	Mudrock	55	1.543	11.632	0.162	1.952	0.093
5	CH1B-5	Mudrock	70	1.567	3.551	0.152	2.113	0.130
6	CH1B-6	Mudrock	90	1.178	0.073	0.159	2.392	0.057
7	CH1B-7	Mudrock	110	0.687	0.061	0.159	2.450	0.049
8	CH1B-8	Mudrock	130	0.702	0.054	0.163	2.440	0.065
9	CH1B-9	Mudrock	150	0.650	0.103	0.152	2.383	0.056
10	CH1B-10	Mudrock	170	0.706	0.112	0.160	2.476	0.054
11	CH1B-11	Mudrock	190	0.601	0.089	0.163	2.518	0.049

Table B.3 continued.

ID #	Sample Name	General Lithology	Outcrop Sample Position (cm)	MgO (wt. %)	CaO (wt. %)	Na_2O (wt. %)	K_2O (wt. %)	P_2O_5 (wt. %)
12	CH1B-12	Mudrock	210	0.667	0.005	0.164	2.448	0.069
13	CH1B-13	Mudrock	230	0.626	0.022	0.157	2.567	0.076
14	CH1B-14	Mudrock	250	0.579	0.064	0.153	2.552	0.063
15	CH1B-15	Mudrock	270	0.710	0.058	0.153	2.314	0.081
16	CH1B-16	Mudrock	290	0.606	0.127	0.159	2.517	0.065
17	CH1B-17	Mudrock	310	0.631	0.206	0.147	2.406	0.076
18	CH1B-18	Mudrock	330	0.501	0.181	0.158	2.401	0.125
19	H/B-1	Mudrock	10	0.728	0.260	0.181	2.452	0.115
20	H/B-2	Mudrock	30	0.617	0.206	0.181	2.273	0.129
21	H/B-2c	Sandstone	35	0.524	0.100	0.243	1.524	0.072
22	H/B-3	Mudrock	60	0.661	0.286	0.171	2.366	0.081
23	H/B-4	Mudrock	70	0.730	1.303	0.168	2.274	0.078
24	H/B-5	Mudrock	90	0.902	0.927	0.174	2.281	0.135
25	H/B-6	Mudrock	110	0.723	0.212	0.182	2.289	0.084
26	H/B-7	Mudrock	125	0.968	0.259	0.171	2.424	0.119
27	H/B-8	Mudrock	145	0.926	0.361	0.164	2.367	0.099
28	H/B-9	Mudrock	160	0.837	0.290	0.168	2.336	0.102
29	H/B-10	Mudrock	175	0.834	0.239	0.164	2.404	0.105
30	H/B-11	Mudrock	195	0.794	0.271	0.157	2.262	0.097
31	H/B-12	Mudrock	215	0.759	0.519	0.151	2.165	0.085
32	H/B-13	Mudrock	270	0.986	0.589	0.167	2.151	0.127
33	H/B-14	Mudrock	290	0.645	0.396	0.170	2.274	0.088
34	H/B-15	Mudrock	320	0.657	1.764	0.170	2.196	0.117
35	H/B-16	Mudrock	350	0.906	0.852	0.177	2.254	0.111
36	H/B-17	Mudrock	365	0.769	1.055	0.166	2.187	0.073
37	H/B-18	Mudrock	375	1.503	27.318	0.138	1.031	0.545
38	H/B-19	Mudrock	410	1.194	43.228	0.093	0.445	0.460
39	H/B-20	Mudrock	450	1.526	27.020	0.109	1.090	0.384
40	H/B-21	Mudrock	490	1.427	28.308	0.094	1.134	0.207
41	H/B-22	Mudrock	560	1.490	21.597	0.122	1.581	0.414
42	H/B-23	Mudrock	590	1.352	28.159	0.104	1.217	0.306
43	UB-1	Mudrock	0	1.473	27.434	0.125	0.981	0.504
44	UB-2	Mudrock	30	1.697	20.584	0.120	1.393	0.292
45	UB-3	Mudrock	80	1.389	32.059	0.110	0.968	0.330
46	UB-Org.	Organics	85	-	-	-	-	-
47	UB-4	Mudrock	115	1.491	17.824	0.140	1.779	0.434
48	UB-5	Mudrock	140	1.339	28.370	0.114	1.205	0.275
49	UB-6	Mudrock	180	1.382	37.127	0.124	0.754	0.745
50	UB-7	Mudrock	200	1.298	30.010	0.100	1.051	0.204
51	UB-8	Mudrock	235	1.155	41.803	0.089	0.672	0.255
52	UB-9	Mudrock	290	1.278	33.455	0.100	0.887	0.355
53	UBDS-1	Mudrock	10	1.315	25.318	0.099	1.081	0.143
54	UBDS-2	Mudrock	30	1.449	20.286	0.116	1.329	0.296
55	UBDS-3	Mudrock	75	1.386	27.148	0.115	1.126	0.277
56	UBDS-4	Mudrock	105	1.295	26.024	0.113	1.252	0.249

Table B.3 continued.

ID #	Sample Name	General Lithology	Outcrop Sample Position (cm)	MgO (wt. %)	CaO (wt. %)	Na_2O (wt. %)	K_2O (wt. %)	P_2O_5 (wt. %)
57	UBDS-5	Mudrock	155	1.281	31.972	0.099	1.118	0.316
58	HD-1	Mudrock	10	1.547	26.999	0.159	1.071	0.319
59	HD-2	Mudrock	30	1.533	23.647	0.209	1.184	0.220
60	HD-3	Mudrock	60	1.430	27.294	0.145	1.134	0.315
61	HD-4	Mudrock	80	1.223	33.609	0.116	0.802	0.315
62	HD-5	Limestone	95	1.158	49.595	0.096	0.149	0.152
63	HD-6	Mudrock	120	1.228	33.190	0.111	0.859	0.215
64	HD-7	Mudrock	135	1.199	31.938	0.103	0.913	0.239
65	HD-8	Limestone	140	2.131	45.409	0.082	0.115	0.055
66	HD-9	Bentonite	145	3.091	6.940	0.132	0.632	0.069
67	HD-10	Limestone	155	1.181	48.596	0.066	0.191	0.191
68	HD-11A	Mudrock	170	1.388	29.495	0.107	1.032	0.153
69	HD-11B	Mudrock	190	1.212	34.365	0.103	0.739	0.308
70	HD-12	Mudrock	225	1.196	33.701	0.090	0.848	0.159
71	HD-13	Limestone	255	1.144	49.373	0.051	0.182	0.061
72	HD-14	Mudrock	265	1.220	31.268	0.101	1.183	0.193
73	HD-15	Bentonite	273	2.468	3.132	0.039	0.102	0.010
74	HD-16	Limestone	287	2.043	47.801	0.034	0.019	0.022
75	HD-17	Mudrock	310	1.446	30.486	0.168	1.032	0.319
76	HD-18	Limestone	333	1.375	51.918	0.050	0.059	0.045
77	HD-19	Mudrock	340	1.554	30.410	0.160	0.963	0.135
78	HD-20	Mudrock	375	1.439	33.843	0.148	0.750	0.127
79	HD-21	Mudrock	395	1.538	30.340	0.149	0.929	0.098
80	HD-22	Mudrock	415	1.647	29.687	0.169	0.895	0.138
81	HD-23	Mudrock	435	1.508	28.591	0.196	0.992	0.126
82	HD-24	Mudrock	465	1.520	32.937	0.156	0.828	0.135
83	HD-25	Mudrock	485	1.690	29.113	0.175	0.988	0.109
84	HD-26	Mudrock	505	1.731	29.334	0.314	1.010	0.119
85	HD-27	Mudrock	525	1.718	27.625	0.209	1.017	0.116
86	HD-28	Mudrock	545	1.820	26.944	0.175	0.997	0.126
87	HD-29	Mudrock	565	1.837	25.582	0.228	1.057	0.115
88	HD-30	Limestone	590	1.195	49.913	0.094	0.188	0.058
89	HD-31	Limestone	600	3.126	28.764	0.180	0.072	0.046
90	HD-32	Mudrock	610	1.520	32.384	0.180	0.787	0.113
91	HD-33	Mudrock	630	1.522	31.647	0.168	0.863	0.194
92	HD-34	Mudrock	650	1.349	36.281	0.153	0.634	0.110
93	HD-35	Mudrock	670	1.462	32.814	0.165	0.738	0.104
94	HD-36	Mudrock	700	1.244	38.998	0.134	0.506	0.140
95	HD-37	Mudrock	710	1.461	30.661	0.164	0.799	0.104
96	HD-38	Mudrock	740	1.367	36.065	0.190	0.573	0.146
97	HD-39	Limestone	755	2.192	45.411	0.119	0.054	0.043
98	HD-40	Mudrock	770	1.380	34.083	0.191	0.647	0.154
99	HD-41	Mudrock	790	1.887	23.969	0.260	0.859	0.111
100	HD-42	Mudrock	820	1.267	37.271	0.148	0.481	0.146
101	HD-43	Limestone	830	1.540	50.047	0.132	0.081	0.047

Table B.3 continued.

ID #	Sample Name	General Lithology	Outcrop Sample Position (cm)	MgO (wt. %)	CaO (wt. %)	Na_2O (wt. %)	K_2O (wt. %)	P_2O_5 (wt. %)
102	HD-44	Limestone	868	1.308	40.643	0.490	0.157	0.352
103	HD-45	Mudrock	905	1.363	36.658	0.237	0.444	0.235
104	HD-46	Limestone	925	1.244	52.950	0.075	0.052	0.048
105	HD-47	Mudrock	950	1.476	33.203	0.227	0.542	0.120
106	HD-48	Limestone	965	2.101	46.814	0.118	0.042	0.046
107	HD-49	Mudrock	985	1.526	35.641	0.330	0.458	0.221
108	HD-50	Mudrock	1005	1.327	38.848	0.188	0.400	0.133
109	HD-51	Mudrock	1050	1.250	41.220	0.165	0.290	0.141
110	HD-52	Mudrock	1090	1.140	41.295	0.152	0.310	0.111
111	HD-53	Mudrock	1155	1.375	43.460	0.184	0.180	0.184
112	HD-54	Mudrock	1170	1.215	39.574	0.168	0.357	0.124
113	HD-55	Mudrock	1195	1.214	39.683	0.127	0.334	0.090
114	HD-56	Limestone	1225	1.237	50.243	0.103	0.045	0.040
115	WPDS-1	Mudrock	10	1.795	28.167	0.321	1.039	0.114
116	WPDS-2	Mudrock	30	1.676	30.327	0.439	0.976	0.115
117	WPDS-3	Limestone	45	2.260	43.214	0.181	0.094	0.041
118	WPDS-4	Mudrock	60	1.465	36.682	0.285	0.684	0.115
119	WPDS-5	Mudrock	80	1.594	29.736	0.319	0.922	0.098
120	WPDS-6	Mudrock	100	1.573	34.822	0.405	0.724	0.131
121	WPDS-7	Mudrock	120	1.629	33.674	0.393	0.725	0.107
122	WPDS-8	Mudrock	125	1.368	39.056	0.217	0.491	0.130
123	WPDS-9	Mudrock	150	1.525	32.490	0.224	0.840	0.114
124	WPDS-10	Mudrock	180	1.588	34.812	0.343	0.646	0.126
125	WPDS-11	Mudrock	200	2.483	19.335	0.530	0.787	0.106
126	WPDS-12	Mudrock	215	1.591	29.743	0.228	0.829	0.116
127	WPDS-13	Limestone	235	1.460	49.741	0.125	0.093	0.035
128	WPDS-14	Mudrock	260	1.470	33.966	0.290	0.632	0.162
129	WPDS-15	Mudrock	270	1.587	31.806	0.335	0.685	0.178
130	WPDS-16	Mudrock	290	1.640	37.516	0.541	0.270	0.376
131	WPDS-17	Mudrock	300	3.593	27.161	0.455	0.187	0.156
132	WPDS-18	Mudrock	320	1.383	38.607	0.348	0.403	0.231
133	WPDS-19	Limestone	340	1.295	52.038	0.126	0.058	0.050
134	WPDS-20	Mudrock	360	2.132	33.297	0.391	0.337	0.236
135	WPDS-21	Mudrock	380	1.608	37.360	0.479	0.396	0.280
136	WPDS-22	Mudrock	400	1.265	40.142	0.220	0.390	0.195
137	WP-1	Mudrock	10	2.040	19.054	0.215	1.398	0.137
138	WP-2	Mudrock	40	2.330	21.660	0.210	1.389	0.122
139	WP-3	Mudrock	60	2.404	10.936	0.581	1.580	0.102
140	WP-4	Limestone	80	2.799	42.067	0.146	0.130	0.066
141	WP-5	Limestone	105	1.908	47.752	0.151	0.129	0.071
142	WP-6	Mudrock	145	1.504	44.394	0.381	0.425	0.197
143	WP-7	Limestone	160	1.269	50.612	0.077	0.113	0.046
144	WP-8	Mudrock	185	1.755	20.783	0.187	1.675	0.084
145	WP-9	Mudrock	200	1.151	45.554	0.117	0.441	0.066
146	WP-10	Mudrock	225	1.551	20.948	0.190	1.887	0.107

Table B.3 continued.

ID #	Sample Name	General Lithology	Outcrop Sample Position (cm)	MgO (wt. %)	CaO (wt. %)	Na_2O (wt. %)	K_2O (wt. %)	P_2O_5 (wt. %)
147	WP-11	Conglomerate	230	1.941	42.603	0.302	0.293	0.359
148	WP-Org.	Organics	230	0.415	1.675	0.233	0.115	0.006
149	WP-12	Mudrock	255	1.455	22.690	0.183	2.103	0.129
150	WP-13	Limestone	270	1.024	48.237	0.097	0.352	0.068
151	WP-14	Bentonite	290	2.811	2.845	0.101	0.254	0.034
152	WP-15	Mudrock	305	1.282	29.162	0.186	1.023	0.541
153	WP-16	Mudrock	310	1.220	35.225	0.240	0.833	0.783
154	WP-17	Limestone	315	1.191	44.959	0.145	0.464	0.245
155	WP-18	Mudrock	330	1.107	26.491	0.207	1.313	0.130
156	C11-1	Mudrock	0	1.277	21.667	0.185	1.723	0.160
157	C11-2	Mudrock	25	1.336	26.397	0.197	1.500	0.242
158	C11-2 Org.	Organics	25	-	-	-	-	-
159	C11-3	Mudrock	40	1.243	24.031	0.208	1.613	0.182
160	C11-4	Mudrock	55	1.173	36.846	0.152	0.914	0.168
161	C11-5	Mudrock	75	1.086	37.240	0.140	0.836	0.159
162	C11-6	Mudrock	90	1.189	44.557	0.153	0.496	0.234
163	EFAC-1	Mudrock	5	1.552	1.637	0.337	2.933	0.095
164	EFAC-2	Mudrock	15	1.505	1.655	0.336	2.966	0.101
165	EFAC-3	Mudrock	25	1.502	1.675	0.323	2.978	0.104
166	EFAC-4	Mudrock	40	1.472	1.606	0.300	2.954	0.099
167	EFAC-5	Mudrock	50	1.502	1.789	0.318	2.939	0.096
168	EFAC-6	Mudrock	70	1.415	1.231	0.289	2.866	0.093
169	EFAC-7	Mudrock	80	1.466	2.181	0.296	2.967	0.112

Table B.4 Trace elements

ID #	Sample Name	General Lithology	Outcrop Sample Position (cm)	As (ppm)	Ba (ppm)	Co (ppm)	Cr (ppm)	Cu (ppm)	Mo (ppm)	Nb (ppm)	Ni (ppm)	Pb (ppm)
1	CH1B-1	Mudrock	5	8	178	9	55	-1	0	15	28	16
2	CH1B-2	Mudrock	15	6	143	4	44	-2	0	13	22	13
3	CH1B-3	Mudrock	30	3	61	1	23	-6	-1	7	8	7
4	CH1B-4	Mudrock	55	9	159	6	53	-1	0	13	29	16
5	CH1B-5	Mudrock	70	15	226	19	92	16	6	16	78	28
6	CH1B-6	Mudrock	90	12	303	27	104	14	3	19	80	25
7	CH1B-7	Mudrock	110	12	286	13	96	41	6	19	54	22
8	CH1B-8	Mudrock	130	11	289	13	98	32	5	18	53	22
9	CH1B-9	Mudrock	150	13	304	15	97	37	5	21	49	22
10	CH1B-10	Mudrock	170	13	301	65	96	24	2	20	61	28
11	CH1B-11	Mudrock	190	12	292	15	91	191	1	21	46	25
12	CH1B-12	Mudrock	210	11	301	27	93	6	1	21	34	22
13	CH1B-13	Mudrock	230	12	311	7	93	9	3	19	45	21

Table B.4 continued

ID #	Sample Name	General Lithology	Outcrop Sample Position (cm)	As (ppm)	Ba (ppm)	Co (ppm)	Cr (ppm)	Cu (ppm)	Mo (ppm)	Nb (ppm)	Ni (ppm)	Pb (ppm)
14	CH1B-14	Mudrock	250	9	308	10	95	17	3	20	46	21
15	CH1B-15	Mudrock	270	11	290	66	94	21	2	19	60	27
16	CH1B-16	Mudrock	290	12	317	10	91	20	3	20	41	21
17	CH1B-17	Mudrock	310	11	295	6	95	12	2	19	40	20
18	CH1B-18	Mudrock	330	11	331	9	83	20	3	21	44	28
19	H/B-1	Mudrock	10	15	300	3	102	3	4	25	35	22
20	H/B-2	Mudrock	30	19	261	2	88	2	4	27	30	25
21	H/B-2c	Sandstone	35	10	181	0	52	-1	0	17	18	12
22	H/B-3	Mudrock	60	16	274	2	92	3	5	24	31	26
23	H/B-4	Mudrock	70	15	244	3	87	3	9	23	29	29
24	H/B-5	Mudrock	90	15	255	2	94	1	8	23	25	25
25	H/B-6	Mudrock	110	13	243	2	86	3	3	21	30	22
26	H/B-7	Mudrock	125	15	274	2	102	9	3	22	28	28
27	H/B-8	Mudrock	145	15	271	3	99	5	4	22	28	28
28	H/B-9	Mudrock	160	14	263	2	95	7	3	22	27	26
29	H/B-10	Mudrock	175	15	267	3	97	7	4	23	29	29
30	H/B-11	Mudrock	195	15	259	30	94	4	4	23	27	26
31	H/B-12	Mudrock	215	14	267	8	90	8	3	23	27	29
32	H/B-13	Mudrock	270	15	259	22	91	5	4	22	22	26
33	H/B-14	Mudrock	290	18	249	20	81	7	4	23	27	22
34	H/B-15	Mudrock	320	12	259	1	76	5	3	22	23	19
35	H/B-16	Mudrock	350	22	268	3	88	8	4	22	24	22
36	H/B-17	Mudrock	365	8	261	3	83	6	6	23	30	19
37	H/B-18	Mudrock	375	15	68	4	49	32	33	8	108	10
38	H/B-19	Mudrock	410	7	2	0	14	8	22	4	63	4
39	H/B-20	Mudrock	450	21	70	9	62	50	51	11	139	12
40	H/B-21	Mudrock	490	21	53	8	56	63	52	17	143	12
41	H/B-22	Mudrock	560	27	98	7	71	62	59	16	173	16
42	H/B-23	Mudrock	590	22	69	3	68	56	47	10	147	13
43	UB-1	Mudrock	0	18	61	12	45	39	49	10	172	11
44	UB-2	Mudrock	30	30	91	16	79	63	66	22	191	16
45	UB-3	Mudrock	80	15	36	2	52	30	29	10	96	8
46	UB-Org.	Organics	85	-	-	-	-	-	-	-	-	-
47	UB-4	Mudrock	115	32	105	14	84	71	98	21	230	16
48	UB-5	Mudrock	140	19	73	5	66	45	52	13	134	11
49	UB-6	Mudrock	180	20	32	5	39	36	48	11	149	9
50	UB-7	Mudrock	200	17	53	7	36	29	67	15	124	11
51	UB-8	Mudrock	235	11	26	0	20	15	28	6	59	5
52	UB-9	Mudrock	290	17	40	6	41	43	45	11	126	9
53	UBDS-1	Mudrock	10	17	61	9	48	57	123	12	219	10
54	UBDS-2	Mudrock	30	24	105	12	70	52	91	16	182	13
55	UBDS-3	Mudrock	75	17	48	3	57	26	28	11	97	9
56	UBDS-4	Mudrock	105	21	49	6	66	55	59	9	143	11
57	UBDS-5	Mudrock	155	19	21	4	50	42	43	11	111	9
58	HD-1	Mudrock	10	17	61	6	54	28	32	13	109	11

Table B.4 continued

ID #	Sample Name	General Lithology	Outcrop Sample Position (cm)	As (ppm)	Ba (ppm)	Co (ppm)	Cr (ppm)	Cu (ppm)	Mo (ppm)	Nb (ppm)	Ni (ppm)	Pb (ppm)
59	HD-2	Mudrock	30	21	68	11	66	42	63	11	166	11
60	HD-3	Mudrock	60	23	52	7	60	51	49	15	160	11
61	HD-4	Mudrock	80	16	29	4	36	32	52	10	121	10
62	HD-5	Limestone	95	6	-28	-2	6	-3	6	3	16	0
63	HD-6	Mudrock	120	16	36	5	39	26	37	15	111	8
64	HD-7	Mudrock	135	18	29	5	40	32	51	11	144	10
65	HD-8	Limestone	140	8	10	-2	2	-10	3	3	-1	6
66	HD-9	Bentonite	145	38	252	7	6	-4	35	11	41	34
67	HD-10	Limestone	155	5	-3	0	5	-4	7	3	10	2
68	HD-11A	Mudrock	170	16	56	6	31	26	40	10	87	9
69	HD-11B	Mudrock	190	14	38	4	33	31	36	11	98	7
70	HD-12	Mudrock	225	12	29	3	23	26	48	11	108	6
71	HD-13	Limestone	255	5	-20	-2	6	-2	9	3	14	2
72	HD-14	Mudrock	265	15	49	3	30	42	51	12	105	8
73	HD-15	Bentonite	273	12	50	-2	5	-6	14	6	9	20
74	HD-16	Limestone	287	9	-32	-4	2	-11	4	2	0	2
75	HD-17	Mudrock	310	13	48	3	28	33	37	11	76	7
76	HD-18	Limestone	333	4	-24	-3	3	-8	3	3	-1	2
77	HD-19	Mudrock	340	12	44	2	24	30	48	12	75	8
78	HD-20	Mudrock	375	11	35	5	18	23	68	10	85	7
79	HD-21	Mudrock	395	14	41	6	22	22	48	14	71	6
80	HD-22	Mudrock	415	14	46	4	20	29	64	15	96	9
81	HD-23	Mudrock	435	16	55	5	24	38	73	14	122	9
82	HD-24	Mudrock	465	11	29	4	20	20	52	12	92	7
83	HD-25	Mudrock	485	14	53	5	23	29	68	16	121	9
84	HD-26	Mudrock	505	12	57	4	23	29	58	16	101	7
85	HD-27	Mudrock	525	13	63	5	22	31	63	19	110	8
86	HD-28	Mudrock	545	14	53	4	23	32	62	18	106	9
87	HD-29	Mudrock	565	16	67	6	25	33	64	18	109	11
88	HD-30	Limestone	590	3	-14	-2	7	-4	14	4	11	1
89	HD-31	Limestone	600	27	36	-8	19	-7	33	3	27	3
90	HD-32	Mudrock	610	12	24	3	18	22	52	14	93	6
91	HD-33	Mudrock	630	12	50	3	21	30	73	16	96	8
92	HD-34	Mudrock	650	9	16	3	14	18	55	12	83	5
93	HD-35	Mudrock	670	11	28	4	19	22	56	13	89	6
94	HD-36	Mudrock	700	9	31	2	15	19	55	11	82	5
95	HD-37	Mudrock	710	12	65	5	19	29	72	16	120	8
96	HD-38	Mudrock	740	10	27	4	15	19	66	12	87	4
97	HD-39	Limestone	755	26	-31	-3	6	-9	26	2	16	0
98	HD-40	Mudrock	770	10	25	4	19	24	60	12	94	6
99	HD-41	Mudrock	790	16	54	6	22	35	65	13	110	9
100	HD-42	Mudrock	820	8	9	5	17	13	44	11	74	5
101	HD-43	Limestone	830	5	-12	-2	1	-7	7	4	9	1
102	HD-44	Limestone	868	12	17	0	7	-5	11	6	18	4
103	HD-45	Mudrock	905	13	2	5	22	19	45	7	102	6

Table B.4 continued

ID #	Sample Name	General Lithology	Outcrop Sample Position (cm)	As (ppm)	Ba (ppm)	Co (ppm)	Cr (ppm)	Cu (ppm)	Mo (ppm)	Nb (ppm)	Ni (ppm)	Pb (ppm)
104	HD-46	Limestone	925	3	-24	-3	3	-7	5	2	5	1
105	HD-47	Mudrock	950	15	21	5	22	40	64	8	130	8
106	HD-48	Limestone	965	10	-15	-3	4	-8	5	2	5	1
107	HD-49	Mudrock	985	14	23	5	14	20	46	7	91	5
108	HD-50	Mudrock	1005	11	16	3	13	24	50	6	66	4
109	HD-51	Mudrock	1050	10	10	2	15	18	39	5	76	5
110	HD-52	Mudrock	1090	11	0	2	15	24	47	5	91	6
111	HD-53	Mudrock	1155	10	-4	1	9	9	29	3	63	3
112	HD-54	Mudrock	1170	12	11	4	14	22	50	5	65	5
113	HD-55	Mudrock	1195	9	-4	1	10	16	44	6	71	4
114	HD-56	Limestone	1225	5	-21	-3	3	-7	6	2	5	1
115	WPDS-1	Mudrock	10	14	59	6	25	31	59	18	101	10
116	WPDS-2	Mudrock	30	12	59	5	22	29	56	15	93	8
117	WPDS-3	Limestone	45	14	-13	-3	9	-6	20	3	13	2
118	WPDS-4	Mudrock	60	10	20	3	16	20	46	12	79	5
119	WPDS-5	Mudrock	80	11	42	6	21	28	62	17	102	7
120	WPDS-6	Mudrock	100	10	35	6	16	23	63	13	94	6
121	WPDS-7	Mudrock	120	11	29	7	19	18	51	11	73	6
122	WPDS-8	Mudrock	125	9	13	3	14	12	48	8	68	4
123	WPDS-9	Mudrock	150	11	41	3	17	28	59	14	88	6
124	WPDS-10	Mudrock	180	11	24	6	19	22	60	11	78	6
125	WPDS-11	Mudrock	200	19	89	7	23	36	77	11	109	13
126	WPDS-12	Mudrock	215	13	37	5	22	34	59	13	102	8
127	WPDS-13	Limestone	235	8	-31	-3	3	-7	7	5	5	1
128	WPDS-14	Mudrock	260	10	31	3	18	24	49	12	86	7
129	WPDS-15	Mudrock	270	12	26	4	21	27	55	12	101	7
130	WPDS-16	Mudrock	290	13	27	2	10	0	21	5	35	4
131	WPDS-17	Mudrock	300	17	-3	2	10	6	19	2	56	17
132	WPDS-18	Mudrock	320	14	16	3	20	18	45	6	94	8
133	WPDS-19	Limestone	340	4	-33	-3	3	-7	6	3	6	1
134	WPDS-20	Mudrock	360	16	-7	3	12	13	35	7	66	7
135	WPDS-21	Mudrock	380	13	17	4	13	14	33	6	68	3
136	WPDS-22	Mudrock	400	10	11	3	14	23	50	6	80	5
137	WP-1	Mudrock	10	16	106	9	61	26	31	17	104	13
138	WP-2	Mudrock	40	44	52	32	60	18	24	15	115	8
139	WP-3	Mudrock	60	9	83	40	301	74	1	14	138	6
140	WP-4	Limestone	80	1	-18	8	49	19	1	1	22	0
141	WP-5	Limestone	105	1	-17	2	20	8	-1	1	2	0
142	WP-6	Mudrock	145	4	53	1	16	0	0	3	6	3
143	WP-7	Limestone	160	1	-20	-3	4	-8	-1	0	-6	0
144	WP-8	Mudrock	185	10	96	9	48	28	3	21	46	10
145	WP-9	Mudrock	200	3	4	-1	11	-2	1	5	7	2
146	WP-10	Mudrock	225	7	95	6	44	25	2	27	31	9
147	WP-11	Conglomerate	230	8	-7	3	17	-3	5	1	6	2
148	WP-Org.	Organics	230	119	15	34	9	48	12	6	161	8

Table B.4 continued

ID #	Sample Name	General Lithology	Outcrop Sample Position (cm)	As (ppm)	Ba (ppm)	Co (ppm)	Cr (ppm)	Cu (ppm)	Mo (ppm)	Nb (ppm)	Ni (ppm)	Pb (ppm)
149	WP-12	Mudrock	255	7	91	6	46	38	4	16	43	8
150	WP-13	Limestone	270	3	-2	-1	8	0	0	6	1	3
151	WP-14	Bentonite	290	14	89	1	5	-7	5	16	10	31
152	WP-15	Mudrock	305	7	51	1	53	10	2	12	24	8
153	WP-16	Mudrock	310	7	34	1	44	5	2	8	29	7
154	WP-17	Limestone	315	5	6	-1	29	4	1	7	4	3
155	WP-18	Mudrock	330	5	79	4	79	29	6	15	57	8
156	C11-1	Mudrock	0	11	109	4	122	32	2	19	69	11
157	C11-2	Mudrock	25	10	103	2	102	29	2	14	61	8
158	C11-2 Org.	Organics	25	-	-	-	-	-	-	-	-	-
159	C11-3	Mudrock	40	9	127	3	125	31	2	20	69	9
160	C11-4	Mudrock	55	8	57	2	64	20	4	10	54	7
161	C11-5	Mudrock	75	6	38	1	61	16	3	10	39	6
162	C11-6	Mudrock	90	7	14	-1	33	7	3	6	26	4
163	EFAC-1	Mudrock	5	9	320	12	83	5	1	51	38	22
164	EFAC-2	Mudrock	15	10	318	12	84	7	1	50	40	23
165	EFAC-3	Mudrock	25	10	316	13	83	6	1	50	39	22
166	EFAC-4	Mudrock	40	9	316	11	82	5	1	51	39	23
167	EFAC-5	Mudrock	50	9	325	12	84	6	0	49	41	22
168	EFAC-6	Mudrock	70	10	314	15	82	9	2	51	73	25
169	EFAC-7	Mudrock	80	11	319	11	86	7	1	48	54	23

Table B. 5 Trace elements part 2

ID #	Sample Name	General Lithology	Outcrop Sample Position (cm)	Rb (ppm)	Sc (ppm)	Sr (ppm)	Th (ppm)	U (ppm)	V (ppm)	Y (ppm)	Zn (ppm)	Zr (ppm)
1	CH1B-1	Mudrock	5	107	20	287	13	2.9	96	29	53	257
2	CH1B-2	Mudrock	15	94	25	313	12	2.9	76	29	44	237
3	CH1B-3	Mudrock	30	52	33	362	7	2.9	35	31	27	187
4	CH1B-4	Mudrock	55	109	22	333	12	3.1	86	27	49	216
5	CH1B-5	Mudrock	70	141	16	172	13	3.6	170	29	73	166
6	CH1B-6	Mudrock	90	171	15	97	19	3.8	189	35	117	156
7	CH1B-7	Mudrock	110	154	13	155	15	4.4	186	25	76	158
8	CH1B-8	Mudrock	130	152	14	114	16	4.5	180	26	70	157
9	CH1B-9	Mudrock	150	155	13	185	17	4.3	186	27	69	179
10	CH1B-10	Mudrock	170	168	18	149	20	4.4	185	29	197	171
11	CH1B-11	Mudrock	190	154	16	105	23	5.5	177	30	119	203
12	CH1B-12	Mudrock	210	146	13	100	10	3.7	179	26	60	182
13	CH1B-13	Mudrock	230	150	11	279	14	3.6	174	27	67	172
14	CH1B-14	Mudrock	250	155	14	231	17	4.0	182	25	77	169
15	CH1B-15	Mudrock	270	148	17	317	18	5.6	169	24	122	165

Table B. 5 continued

ID #	Sample Name	General Lithology	Outcrop Sample Position (cm)	Rb (ppm)	Sc (ppm)	Sr (ppm)	Th (ppm)	U (ppm)	V (ppm)	Y (ppm)	Zn (ppm)	Zr (ppm)
16	CH1B-16	Mudrock	290	152	13	250	17	3.8	179	24	59	166
17	CH1B-17	Mudrock	310	142	14	280	17	3.6	181	25	56	177
18	CH1B-18	Mudrock	330	143	15	590	20	3.8	163	24	56	169
19	H/B-1	Mudrock	10	149	13	135	13	4.0	198	28	42	215
20	H/B-2	Mudrock	30	143	13	97	13	3.4	179	29	38	266
21	H/B-2c	Sandstone	35	68	9	53	9	3.9	90	31	25	540
22	H/B-3	Mudrock	60	145	11	94	11	3.9	188	25	39	239
23	H/B-4	Mudrock	70	143	17	103	10	3.8	174	26	37	207
24	H/B-5	Mudrock	90	149	17	151	13	3.8	179	26	37	214
25	H/B-6	Mudrock	110	134	12	82	12	4.0	165	28	36	257
26	H/B-7	Mudrock	125	155	13	105	16	4.0	199	25	42	183
27	H/B-8	Mudrock	145	152	13	95	14	4.1	194	24	42	178
28	H/B-9	Mudrock	160	144	13	89	14	3.9	193	25	42	207
29	H/B-10	Mudrock	175	152	12	96	16	4.0	200	24	41	185
30	H/B-11	Mudrock	195	148	12	96	14	4.0	194	24	38	186
31	H/B-12	Mudrock	215	147	13	94	13	3.6	186	25	39	201
32	H/B-13	Mudrock	270	151	12	128	10	3.6	185	23	39	187
33	H/B-14	Mudrock	290	137	14	87	11	5.3	171	24	38	203
34	H/B-15	Mudrock	320	129	12	107	14	5.1	168	23	37	195
35	H/B-16	Mudrock	350	138	15	136	11	5.7	173	20	41	197
36	H/B-17	Mudrock	365	141	14	145	12	8.4	195	22	44	178
37	H/B-18	Mudrock	375	61	31	524	7	13.7	170	34	104	86
38	H/B-19	Mudrock	410	20	40	537	3	11.7	115	16	65	36
39	H/B-20	Mudrock	450	64	32	415	6	18.9	454	19	164	90
40	H/B-21	Mudrock	490	60	34	341	4	19.6	648	14	176	97
41	H/B-22	Mudrock	560	76	30	369	6	19.8	555	22	160	96
42	H/B-23	Mudrock	590	60	35	403	6	15.2	526	17	155	83
43	UB-1	Mudrock	0	60	34	474	7	13.0	386	24	112	87
44	UB-2	Mudrock	30	75	26	313	6	10.4	614	21	183	128
45	UB-3	Mudrock	80	47	34	475	4	10.4	301	18	79	65
46	UB-Org.	Organics	85	-	-	-	-	-	-	-	-	-
47	UB-4	Mudrock	115	76	29	311	7	17.7	990	24	255	115
48	UB-5	Mudrock	140	57	31	434	5	9.6	525	16	150	84
49	UB-6	Mudrock	180	35	38	566	4	16.4	343	25	225	66
50	UB-7	Mudrock	200	52	34	390	7	10.6	496	15	123	96
51	UB-8	Mudrock	235	23	40	544	1	8.7	259	15	85	68
52	UB-9	Mudrock	290	42	36	501	3	11.5	476	25	107	111
53	UBDS-1	Mudrock	10	64	33	299	5	9.4	766	11	221	96
54	UBDS-2	Mudrock	30	66	28	316	5	11.9	685	17	198	120
55	UBDS-3	Mudrock	75	53	29	399	5	8.2	305	14	82	77
56	UBDS-4	Mudrock	105	56	31	353	4	11.1	609	15	325	70
57	UBDS-5	Mudrock	155	47	34	469	5	11.1	453	14	111	75
58	HD-1	Mudrock	10	60	32	594	6	8.9	311	18	85	82

Table B. 5 continued

ID #	Sample Name	General Lithology	Outcrop Sample Position (cm)	Rb (ppm)	Sc (ppm)	Sr (ppm)	Th (ppm)	U (ppm)	V (ppm)	Y (ppm)	Zn (ppm)	Zr (ppm)
59	HD-2	Mudrock	30	68	29	437	5	9.9	542	15	138	86
60	HD-3	Mudrock	60	51	33	523	4	11.6	462	16	148	88
61	HD-4	Mudrock	80	38	38	505	4	11.3	419	13	118	62
62	HD-5	Limestone	95	10	44	362	1	4.8	81	4	26	19
63	HD-6	Mudrock	120	40	37	509	4	9.3	295	14	93	74
64	HD-7	Mudrock	135	38	36	529	5	10.7	405	15	176	77
65	HD-8	Limestone	140	8	39	233	3	3.2	22	4	22	50
66	HD-9	Bentonite	145	34	14	485	26	3.3	318	4	145	206
67	HD-10	Limestone	155	9	44	350	2	6.7	52	11	23	33
68	HD-11A	Mudrock	170	47	34	507	5	8.5	291	16	137	107
69	HD-11B	Mudrock	190	38	36	560	2	12.0	374	24	89	102
70	HD-12	Mudrock	225	42	36	502	5	8.9	464	13	121	71
71	HD-13	Limestone	255	11	40	357	1	4.3	72	3	25	21
72	HD-14	Mudrock	265	40	34	516	6	11.3	504	19	99	80
73	HD-15	Bentonite	273	3	8	487	57	7.8	71	1	18	180
74	HD-16	Limestone	287	1	39	190	5	3.6	3	6	13	21
75	HD-17	Mudrock	310	41	34	628	4	13.0	397	18	80	82
76	HD-18	Limestone	333	5	43	238	1	3.7	52	2	16	15
77	HD-19	Mudrock	340	43	35	548	3	7.5	332	14	82	88
78	HD-20	Mudrock	375	34	36	597	4	9.0	198	11	70	60
79	HD-21	Mudrock	395	43	33	557	5	8.2	155	11	67	71
80	HD-22	Mudrock	415	38	35	519	5	9.7	408	12	109	81
81	HD-23	Mudrock	435	41	33	554	5	9.1	461	11	131	78
82	HD-24	Mudrock	465	39	37	631	5	8.3	295	11	85	67
83	HD-25	Mudrock	485	44	33	625	5	8.7	394	11	101	82
84	HD-26	Mudrock	505	44	31	632	5	9.0	419	13	101	84
85	HD-27	Mudrock	525	45	31	572	6	10.7	386	13	100	101
86	HD-28	Mudrock	545	44	31	535	5	10.3	382	12	104	100
87	HD-29	Mudrock	565	47	30	517	6	8.8	424	11	110	101
88	HD-30	Limestone	590	10	42	364	1	3.4	48	5	24	23
89	HD-31	Limestone	600	5	29	276	2	2.7	59	1	24	33
90	HD-32	Mudrock	610	36	34	603	5	8.9	291	13	86	75
91	HD-33	Mudrock	630	41	36	799	5	9.9	448	13	117	81
92	HD-34	Mudrock	650	30	35	637	3	7.9	300	10	74	60
93	HD-35	Mudrock	670	37	36	582	5	8.6	223	11	69	72
94	HD-36	Mudrock	700	25	36	610	2	9.7	250	11	76	57
95	HD-37	Mudrock	710	38	33	535	4	9.8	442	10	99	76
96	HD-38	Mudrock	740	28	36	644	3	10.6	213	12	69	61
97	HD-39	Limestone	755	3	41	186	1	5.3	47	3	15	16
98	HD-40	Mudrock	770	31	36	676	4	9.7	252	14	85	66
99	HD-41	Mudrock	790	38	32	494	6	9.5	458	9	112	91
100	HD-42	Mudrock	820	25	36	617	3	9.8	135	13	67	63
101	HD-43	Limestone	830	4	42	237	3	5.8	109	7	18	28

Table B. 5 continued

ID #	Sample Name	General Lithology	Outcrop Sample Position (cm)	Rb (ppm)	Sc (ppm)	Sr (ppm)	Th (ppm)	U (ppm)	V (ppm)	Y (ppm)	Zn (ppm)	Zr (ppm)
102	HD-44	Limestone	868	4	36	618	3	9.4	25	22	37	79
103	HD-45	Mudrock	905	18	36	619	5	12.7	194	16	80	63
104	HD-46	Limestone	925	3	43	297	0	3.2	66	1	19	19
105	HD-47	Mudrock	950	22	36	525	4	11.4	512	9	113	71
106	HD-48	Limestone	965	2	40	265	2	2.4	41	1	16	20
107	HD-49	Mudrock	985	21	35	587	3	9.8	260	12	73	56
108	HD-50	Mudrock	1005	21	39	648	3	8.9	257	9	72	50
109	HD-51	Mudrock	1050	14	37	680	2	5.9	336	7	88	43
110	HD-52	Mudrock	1090	17	40	678	1	6.1	352	7	95	40
111	HD-53	Mudrock	1155	8	40	734	2	6.7	165	9	67	38
112	HD-54	Mudrock	1170	20	35	627	4	8.9	221	8	81	45
113	HD-55	Mudrock	1195	20	35	579	3	7.7	342	8	88	45
114	HD-56	Limestone	1225	2	41	265	1	3.3	53	4	19	15
115	WPDS-1	Mudrock	10	44	30	727	6	8.8	348	12	107	92
116	WPDS-2	Mudrock	30	42	33	683	5	9.1	292	12	110	79
117	WPDS-3	Limestone	45	6	39	260	0	4.2	60	2	16	23
118	WPDS-4	Mudrock	60	31	36	692	2	8.4	247	11	85	65
119	WPDS-5	Mudrock	80	39	33	654	7	8.3	424	10	96	81
120	WPDS-6	Mudrock	100	32	33	711	4	8.4	342	10	120	66
121	WPDS-7	Mudrock	120	33	33	588	4	8.4	149	10	56	67
122	WPDS-8	Mudrock	125	25	38	731	2	8.7	139	11	56	50
123	WPDS-9	Mudrock	150	37	32	620	5	9.7	419	10	99	71
124	WPDS-10	Mudrock	180	32	35	630	3	10.1	157	13	71	63
125	WPDS-11	Mudrock	200	34	26	564	8	9.6	388	10	106	97
126	WPDS-12	Mudrock	215	36	31	599	4	8.8	374	11	112	78
127	WPDS-13	Limestone	235	5	43	247	2	5.1	46	5	20	27
128	WPDS-14	Mudrock	260	29	35	641	2	10.5	284	13	105	73
129	WPDS-15	Mudrock	270	31	34	573	4	11.6	261	16	89	83
130	WPDS-16	Mudrock	290	9	37	679	4	11.7	51	27	39	90
131	WPDS-17	Mudrock	300	7	31	675	12	8.6	124	17	75	139
132	WPDS-18	Mudrock	320	16	36	673	1	11.8	196	17	90	57
133	WPDS-19	Limestone	340	4	44	321	2	3.2	69	2	34	18
134	WPDS-20	Mudrock	360	14	33	586	4	7.5	188	12	47	76
135	WPDS-21	Mudrock	380	15	33	676	2	8.7	185	10	57	50
136	WPDS-22	Mudrock	400	20	37	678	2	9.7	203	9	82	49
137	WP-1	Mudrock	10	80	25	486	7	9.2	434	16	130	97
138	WP-2	Mudrock	40	56	31	482	6	5.6	256	16	75	78
139	WP-3	Mudrock	60	41	36	405	6	3.4	255	13	74	116
140	WP-4	Limestone	80	5	44	246	0	2.4	74	17	24	19
141	WP-5	Limestone	105	6	43	214	0	2.0	44	15	23	17
142	WP-6	Mudrock	145	13	41	789	2	2.8	17	28	24	68
143	WP-7	Limestone	160	5	45	247	0	3.3	10	13	15	17
144	WP-8	Mudrock	185	64	31	433	5	3.8	145	14	58	109

Table B. 5 continued

ID #	Sample Name	General Lithology	Outcrop Sample Position (cm)	Rb (ppm)	Sc (ppm)	Sr (ppm)	Th (ppm)	U (ppm)	V (ppm)	Y (ppm)	Zn (ppm)	Zr (ppm)
145	WP-9	Mudrock	200	15	42	752	2	2.3	38	12	23	28
146	WP-10	Mudrock	225	63	28	453	5	3.8	126	14	62	132
147	WP-11	Conglomerate	230	6	38	713	0	2.4	24	12	20	22
148	WP-Org.	Organics	230	2	5	127	-2	4.4	1901	0	128	428
149	WP-12	Mudrock	255	56	29	455	6	3.4	172	12	71	96
150	WP-13	Limestone	270	14	41	540	2	3.5	22	9	19	27
151	WP-14	Bentonite	290	8	7	317	73	4.1	17	4	87	169
152	WP-15	Mudrock	305	33	31	629	5	6.9	112	38	78	94
153	WP-16	Mudrock	310	26	36	763	2	7.5	87	46	69	72
154	WP-17	Limestone	315	18	43	724	1	2.6	53	17	36	40
155	WP-18	Mudrock	330	50	30	526	4	3.5	162	10	71	83
156	C11-1	Mudrock	0	76	31	364	7	4.3	228	16	80	119
157	C11-2	Mudrock	25	58	34	498	5	4.6	230	19	101	107
158	C11-2 Org.	Organics	25	-	-	-	-	-	-	-	-	-
159	C11-3	Mudrock	40	69	29	409	7	5.1	266	17	77	123
160	C11-4	Mudrock	55	36	38	605	4	4.2	252	14	105	72
161	C11-5	Mudrock	75	36	38	558	3	4.3	229	14	96	72
162	C11-6	Mudrock	90	23	40	796	3	3.7	121	12	43	44
163	EFAC-1	Mudrock	5	159	15	321	17	3.9	185	28	81	231
164	EFAC-2	Mudrock	15	158	13	308	18	3.7	185	28	83	231
165	EFAC-3	Mudrock	25	160	15	298	16	4.0	186	29	76	232
166	EFAC-4	Mudrock	40	159	15	307	17	4.1	188	27	74	229
167	EFAC-5	Mudrock	50	158	15	314	17	4.3	185	27	90	228
168	EFAC-6	Mudrock	70	163	13	237	18	4.2	197	24	88	236
169	EFAC-7	Mudrock	80	156	15	294	17	4.6	196	23	76	225

REFERENCES

Adams, J. A., and C. E. Weaver, 1958, Thorium-to-uranium ratios as indicators of sedimentary processes: example of concept of geochemical facies: AAPG Bulletin, v. 42, no. 2, p. 387–430.

Adkins, W. S., and F. E. Lozo, 1951, Stratigraphy of the Woodbine and Eagle Ford, Waco area, Texas: East Texas Geological Society, p. 101–161.

Arthur, M. A., W. E. Dean, and L. M. Pratt, 1988, Geochemical and climatic effects of increased marine organic carbon burial at the Cenomanian/Turonian boundary: Nature, v. 335, no. 6192, p. 714–717.

Arthur, M. A., and B. B. Sageman, 2005, Sea-level control on source-rock development: perspectives from the Holocene Black Sea, the mid-Cretaceous Western Interior Basin of North America, and the Late Devonian Appalachian Basin: SEPM Special Publication, v. 82, p. 35–59.

Berner, R. A., 1982, Burial of organic carbon and pyrite sulfur in the modern ocean: its geochemical and environmental significance: American Journal of Science, v. 282, no. 4, p. 451–473.

Bice, K. L., D. Birgel, P. A. Meyers, K. A. Dahl, K.-U. Hinrichs, and R. D. Norris, 2006, A multiple proxy and model study of Cretaceous upper ocean temperatures and atmospheric CO2 concentrations: Paleoceanography, v. 21, no. 2, p. PA2002.

Blakey, R., 1994, Global Paleogeography: <http://www2.nau.edu/rcb7/nam.html> (accessed February 12, 2013).

Brumsack, H.-J., 2006, The trace metal content of recent organic carbon-rich sediments: Implications for Cretaceous black shale formation: Palaeogeography, Palaeoclimatology, Palaeoecology, v. 232, no. 2-4, p. 344–361.

Byerly, G. R., 1991, Igneous activity, *in* The Geology of North America: Geological Society of America, The Gulf of Mexico basin: Boulder, Colorado, p. 191–108.

Calvert, S. ., and T. . Pedersen, 1993, Geochemistry of Recent oxic and anoxic marine sediments: Implications for the geological record: Marine Sediments, Burial, Pore Water Chemistry, Microbiology and Diagenesis, v. 113, no. 1–2, p. 67–88.

Canfield, D. E., 1994, Factors influencing organic carbon preservation in marine sediments: Chemical Geology, v. 114, no. 3–4, p. 315–329.

Van Cappellen, P., and E. D. Ingall, 1994, Benthic phosphorus regeneration, net primary production, and ocean anoxia: A model of the coupled marine biogeochemical cycles of carbon and phosphorus: Paleoceanography, v. 9, no. 5, p. 677–692.

Charvat, W. A., 1985, The nature and origin of the bentonite rich Eagle Ford rocks, central Texas, Thesis: Baylor University.

Dawson, W. C., 1997, Limestone microfacies and sequence stratigraphy: Eagle Ford Group (Cenomanian-Turonian) north-central Texas outcrops: Gulf Coast Association of Geological Societies Transactions, v. XLVII, p. 99–106.

Dawson, W. C., 2000, Shale microfacies: Eagle Ford Group (Cenomanian-Turonian) north-central Texas outcrops and subsurface equivalents: Gulf Coast Association of Geological Societies Transactions, v. 50, p. 607–621.

Dawson, W. C., and W. R. Almon, 2010, Eagle Ford Shale Variability: Sedimentologic Influences on Source and Reservoir Character in an Unconventional Resource Unit: Gulf Coast Association of Geological Societies Transactions, v. 60, p. 181–190.

Donovan, A. D., and T. S. Staerker, 2010, Sequence Stratigraphy of the Eagle Ford (Boquillas) Formation in the Subsurface of South Texas and Outcrops of West Texas: Gulf Coast Association of Geological Societies Transactions, v. 60, p. 861–899.

Freeman, V. L., 1961, Contact of Boquillas Flags and Austin Chalk in Val Verde and Terrell Counties, Texas: Geological Notes: AAPG Bulletin, v. 45, no. 1, p. 105–107.

Froelich, P. N., G. P. Klinkhammer, M. L. Bender, N. A. Luedtke, G. R. Heath, D. Cullen, P. Dauphin, D. Hammond, B. Hartman, and V. Maynard, 1979, Early oxidation of organic matter in pelagic sediments of the eastern equatorial Atlantic: suboxic diagenesis: Geochimica et Cosmochimica Acta, v. 43, no. 7, p. 1075–1090.

Galloway, W. E., 2008, Chapter 15 Depositional Evolution of the Gulf of Mexico Sedimentary Basin, *in* Andrew D. Miall, ed., Sedimentary Basins of the World: Elsevier, p. 505–549.

Haq, B. U., J. Hardenbol, and P. R. Vail, 1987, Chronology of Fluctuating Sea Levels since the Triassic: Science, v. 235, no. 4793, p. 1156–1167.

Hartnett, H. E., R. G. Keil, J. I. Hedges, and A. H. Devol, 1998, Influence of oxygen exposure time on organic carbon preservation in continental margin sediments: Nature, v. 391, no. 6667, p. 572–575.

Helz, G. R., C. V. Miller, J. M. Charnock, J. F. W. Mosselmans, R. A. D. Pattrick, C. D. Garner, and D. J. Vaughan, 1996, Mechanism of molybdenum removal from the sea and its concentration in black shales: EXAFS evidence: Geochimica et Cosmochimica Acta, v. 60, no. 19, p. 3631–3642.

Hentz, T. F., and S. C. Ruppel, 2010, Regional Lithostratigraphy of the Eagle Ford Shale: Maverick Basin to East Texas Basin: Gulf Coast Association of Geological Societies Transactions, v. 60, p. 325–337.

Hsu, S.-C., and P. P. Nelson, 2002, Characterization of eagle ford shale: Engineering Geology, v. 67, no. 1, p. 169–183.

Hunter, B. E., and D. K. Davies, 1979, Distribution of Volcanic sediments in the Gulf Coastal Province--Significance to Petroleum Geology: Houston Geological Society Bullitin, v. 29, p. 147–155.

Ingall, E., and R. Jahnke, 1997, Influence of water-column anoxia on the elemental fractionation of carbon and phosphorus during sediment diagenesis: Marine Geology, v. 139, no. 1, p. 219–229.

Jenkyns, H. C., 2010, Geochemistry of oceanic anoxic events: Geochemistry, Geophysics, Geosystems, v. 11, no. 3, p. 1–30.

Jiang, M. J., 1989, Biostratigraphy and geochronology of the Eagle Ford Shale, Austin Chalk, and lower Taylor marl in Texas based on calcareous nanofossils, Ph.D. dissertation: Texas A&M University.

Junium, C. K., and M. A. Arthur, 2007, Nitrogen cycling during the Cretaceous, Cenomanian-Turonian Oceanic Anoxic Event II: Geochemistry, Geophysics, Geosystems, v. 8, no. 3, p. 1–18.

Karl, D., A. Michaels, B. Bergman, D. Capone, E. Carpenter, R. Letelier, F. Lipschultz, H. Paerl, D. Sigman, and L. Stal, 2002, Dinitrogen fixation in the world’s oceans: Biogeochemistry, v. 57/58, p. 47–98.

Kearns, T. J., 2012, Chemostratigraphy of the Eagle Ford formation, Masters Thesis: University of Texas at Arlington, 270 p.

Kryc, K. A., R. W. Murray, and D. W. Murray, 2003, Al-to-oxide and Ti-to-organic linkages in biogenic sediment: relationships to paleo-export production and bulk Al/Ti: Earth and Planetary Science Letters, v. 211, no. 1-2, p. 125–141.

Kuypers, M. M., Y. van Breugel, S. Schouten, E. Erba, and J. S. S. Damsté, 2004, N2-fixing cyanobacteria supplied nutrient N for Cretaceous oceanic anoxic events: Geology, v. 32, no. 10, p. 853–856.

Liro, L. M., W. C. Dawson, B. J. Katz, and V. D. Robison, 1994, Sequence Stratigraphic Elements and Geochemical Variability within a“ Condensed Section”: Eagle Ford Group, East-Central Texas: Gulf Coast Association of Geological Societies Transactions, v. 44, p. 393–402.

Lock, B. E., and L. Peschier, 2006, Boquillas (Eagle Ford) Upper Slope Sediments, West Texas: Outcrop Analogs for Potential Shale Reservoirs: Gulf Coast Association of Geological Societies Transactions, v. 56, p. 491–508.

Magoon, L. B., 1987, Petroleum Systems of the United States: United States Government Printing Office, Washington, Petroleum Systems of the United States U.S. Geological Survey Bulletin 1870.

Martin, R., S. P. E. Jason Baihly, S. P. E. Raj Malpani, and S. P. E. Garrett Lindsay, 2011, Understanding Production from Eagle Ford-Austin Chalk System, *in* Denver, Colorado, USA: Society of Petroleum Engineers.

Meyers, P. A., S. M. Bernasconi, and A. Forster, 2006, Origins and accumulation of organic matter in expanded Albian to Santonian black shale sequences on the Demerara Rise, South American margin: Organic Geochemistry, v. 37, no. 12, p. 1816–1830.

Meyers, S. R., B. B. Sageman, and L. A. Hinnov, 2001, Integrated quantitative stratigraphy of the Cenomanian-Turonian Bridge Creek Limestone Member using evolutive harmonic analysis and stratigraphic modeling: Journal of Sedimentary Research, v. 71, no. 4, p. 628–644.

Meyers, S. R., B. B. Sageman, and T. W. Lyons, 2005, Organic carbon burial rate and the molybdenum proxy: Theoretical framework and application to Cenomanian-Turonian oceanic anoxic event 2: Paleoceanography, v. 20, no. 2.

Moran, L., 2013, High Resolution Geochemistry Of The Cretaceous Eagle Ford Shale, Bee County, Texas, Masters Thesis: University of Texas at Arlington, 56 p.

Pedersen, T. F., and S. E. Calvert, 1990, Anoxia vs. Productivity: What Controls the Formation of Organic-Carbon-Rich Sediments and Sedimentary Rocks?: AAPG Bulletin, v. 74, no. 4, p. 454–466.

Piper, D. Z., and S. E. Calvert, 2009, A marine biogeochemical perspective on black shale deposition: Earth-Science Reviews, v. 95, no. 1–2, p. 63–96.

Pratt, L. M., E. R. Force, and B. Pomerol, 1991, Coupled manganese and carbon-isotopic events in marine carbonates at the Cenomanian-Turonian boundary: Journal of Sedimentary Research, v. 61, no. 3, p. 370–383.

Pratt, L. M., and C. N. Threlkeld, 1984, Stratigraphic significance of 13C/12C ratios in mid-Cretaceous rocks of the Western Interior, USA: Canadian Society of Petroleum Geologists, v. 9, p. 305–312.

Ratcliffe, K. T., A. M. Wright, P. Montgomery, A. Palfrey, A. Vonk, J. Vermeulen, and M. Barrett, 2010, Application of chemostratigraphy to the Mungaroo Formation, the Gorgon Field, offshore Northwest Australia: APPEA Journal, p. 371–385.

Ratcliffe, K. T., A. M. Wright, and K. Schmidt, 2012, Application of inorganic whole-rock geochemistry to shale resource plays: an example from the Eagle Ford Shale Formation, Texas: The Sedimentary Record, v. 10, no. 2, p. 4–9.

Sachs, J. P., and D. J. Repeta, 1999, Oligotrophy and nitrogen fixation during eastern Mediterranean sapropel events: Science, v. 286, no. 5449, p. 2485–2488.

Sageman, B. B., A. E. Murphy, J. P. Werne, C. A. Ver Straeten, D. J. Hollander, and T. W. Lyons, 2003, A tale of shales: the relative roles of production, decomposition, and dilution in the accumulation of organic-rich strata, Middle–Upper Devonian, Appalachian basin: Chemical Geology, v. 195, no. 1-4, p. 229–273.

Schlanger, S., and H. Jenkyns, 1976, Cretaceous oceanic anoxic events: causes and consequences: Geologie en mijnbouw, v. 55, no. 3-4, p. 179–184.

Seibold, E., and W. H. Berger, 1996, The Sea Floor: An Introduction to Marine Geology: Springer.

Stehli, F. G., W. B. Creath, C. F. Upshaw, and J. M. Forgotson, 1972, Depositional history of Gulfian Cretaceous of east Texas embayment: AAPG Bulletin, v. 56, no. 1, p. 38–67.

Stephenson, L. W., 1929, Unconformities in upper Cretaceous series of Texas: AAPG Bulletin, v. 13, no. 10, p. 1323–1334.

Surles, M. A., 1986, Stratigraphy of the Eagle Ford Group (Upper Cretaceous) and its source-rock potential in the East Texas Basin: Baylor Geological Studies Bulletin.

Sverdrup, H. U., M. W. Johnson, and R. H. Fleming, 1942, The oceans: their physics, chemistry, and general biology: Prentice-Hall New York.

Tribovillard, N., T. J. Algeo, T. Lyons, and A. Riboulleau, 2006, Trace metals as paleoredox and paleoproductivity proxies: An update: Chemical Geology, v. 232, no. 1-2, p. 12–32.

Tribovillard, N., V. Bout-Roumazeilles, T. Algeo, T. W. Lyons, T. Sionneau, J. C. Montero-Serrano, A. Riboulleau, and F. Baudin, 2008, Paleodepositional conditions in the Orca Basin as inferred from organic matter and trace metal contents: Marine Geology, v. 254, no. 1-2, p. 62–72.

Turgeon, S. C., and R. A. Creaser, 2008, Cretaceous oceanic anoxic event 2 triggered by a massive magmatic episode: Nature, v. 454, no. 7202, p. 323–326.

Tyson, R. V., and T. H. Pearson, 1991, Modern and ancient continental shelf anoxia: an overview: Geological Society, London, Special Publications, v. 58, no. 1, p. 1–24.

Veizer, J., Y. Godderis, and L. M. Francois, 2000, Evidence for decoupling of atmospheric CO2 and global climate during the Phanerozoic eon: Nature, v. 408, no. 6813, p. 698–701.

Wedepohl, K., 1971, Environmental influences on the chemical composition of shales and clays: Physics and Chemistry of the Earth, v. 8, p. 305–333.

Wedepohl, K. H., 1991, The composition of the upper earth's crust and the natural cycles of selected metals. Metals in natural raw materials: Metals and Their Compounds in the Environment. Occurrence, Analysis, and Biological Relevance, p. 3–17.

Van der Weijden, C. H., 2002, Pitfalls of normalization of marine geochemical data using a common divisor: Marine Geology, v. 184, no. 3, p. 167–187.

Wescott, W. A., and W. C. Hood, 1994, Hydrocarbon generation and migration routes in the East Texas Basin: AAPG bulletin, v. 78, no. 2, p. 287–306.